WELDABILITY AND CORROSION TEST ON BOILER GRADE STEEL (SA-387 Gr-11)

A DISSERTATION

*Submitted in partial fulfillment of the
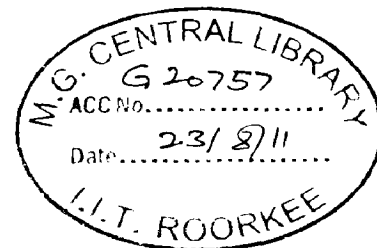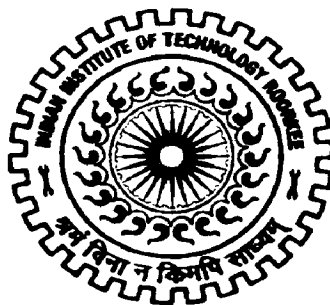requirements for the award of the degree*
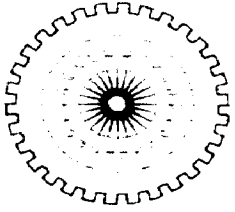*of*
MASTER OF TECHNOLOGY
in
MECHANICAL ENGINEERING
(With Specialization in Welding Engineering)

By
ABHISHEK KUMAR YADAV

**DEPARTMENT OF MECHANICAL AND INDUSTRIAL ENGINEERING
INDIAN INSTITUTE OF TECHNOLOGY ROORKEE
ROORKEE - 247 667 (INDIA)
JUNE, 2011**

INDIAN INSTITUTE OF TECHNOLOGY, ROORKEE

ROORKEE

CANDIDATE'S DECLARATION

I hereby declare that the work being presented in the dissertation report entitled, **"WELDABILITY AND CORROSION TEST ON BOILER GRADE STEEL (SA-387 Gr-11)"**, submitted in the partial fulfillment of the requirements for the award of the degree of Master of Technology in "Mechanical Engineering" with specialization in Welding Engineering, in the Department of Mechanical and Industrial Engineering, Indian Institute of Technology, Roorkee (India) under the supervision and guidance of Ajai Agarwal, Assistant professor, Department of Mechanical & Industrial Engineering and Dr. Devendra Puri, Assistant Professor, Department of Metallurgical and Material Science Engineering.

The matter presented in this seminar has not been submitted by me for the award of any other degree.

Place: Roorkee

Abhishek Kr. Yadav

Dated:30/06/2011   (ABHISHEK KUMAR YADAV)

CERTIFICATE

This is to certify that the above statement made by the candidate is correct to the best of my knowledge.

(Ajai Agrawal)
Assistant Professor
MIED
IIT Roorkee

Dr. Devendra Puri
Assistant Professor
MMED
IIT Roorkee

ACKNOWLEDGEMENT

(ABHISHEK KUMAR YADAV)

ABSTRACT

Welding process involves melting and subsequent cooling and the result of this thermal cycle causes residual stress and degradation of mechanical properties in weldments, when welding thicker sections. In thicker section like pressure vessels, boilers which are used in petrochemical, chemical oil & gas industries the existence of residual stress and un desirable mechanical properties are unacceptable as per critically of these structures.

In the present work the effect of welding current when voltage remain constant at different parameter and after that Mechanical and microstructural properties of Chromium-Molybdenum alloy steel of ASTM A 387 Gr-11 alloy steel is determined, which is commonly used in boilers, pressure vessels, heat exchangers, turbine parts etc. The regions in the weldment like base metal, HAZ and weld metal were studied, through the results obtained from the tensile test, Hardness measurement, Charpy-V-Notch impact test, Microstructural characterization using SEM and optical microscope and chemical analysis using E-DAX. It is concluded that the degradation of mechanical properties of steel is due to the changes that occurred in the microsture.

Material degradation at high temperature is a serious problem in power plants, which encounter severe corrosion problems resulting in the substantial loss. The problems become more prominent as the power plants getting older. The boiler tubes used for super heaters and reheaters in the steam generating systems are subjected to corrosion, resulting in tube wall thinning and premature failure. Hot corrosion has been identified as a serious problem in high temperature applications such as boilers, gas turbines, diesel engines, coal gasification plants and chemical plants.

The present has been performed to evaluate the hot corrosion behavior of chromium-molybdenum alloy steel when exposed to high temperature oxidation in air environment, under isothermal conditions at a temperature of 900^0C, in actual degrading conditions prevailing in a coal fired boiler of a thermal plant. The work is focused on Base metal and weld metal. Isothermal treatment resulted in parabolic oxidation kinetics and thus resulted in weight gain.

CONTENTS

CHAPTER 4   EXPERIMENTATION   22-40

LIST OF FIGURES

LIST OF TABLES

ABBREVIATIONS

Word	Description
PWHT	Post weld heat treatment
HSLA	High strength low alloy steels
SMAW	Shielded metal arc welding
Cr-Mo	Chromium-molybdenum
BM	Base metal
WM	Weld metal
HAZ	Heat affected zone
CGHAZ	Coarse grain Heat affected zone
ROA	Reduction of area
EAF	Elongation of fracture
SEM	Scanning Electron Microscopy
E-DAX	Electron Dispersive Analysis
VHN	Vickers Hardness number
Temp	Temperature
H or h	Hours
V	Arc voltage
I	Welding current
D.C.	Direct current
E	Young's modulus

INTRODUCTION

The components in power boilers and the associated piping's are involved in the following functions:

• Generating steam

• High steam temperature and pressure

• Moving water and steam

Because the tubing and piping systems are multifunctional and operate at different pressures and temperatures, it is reasonable that the components involved are manufactured from different alloys using a range of fabrication techniques. Moreover, because the design conditions of different boilers vary within a broad power-generating system, many different alloys will be used in various product forms. The materials used and the associated product quality checks are covered by applicable specifications and standards. However, it is frequently necessary for utility engineers to have access to basic metallurgical information to aid decision making for specific projects. Maintaining accurate knowledge of the full range of boiler materials is becoming an increasing challenge for two main reasons: the information base continues to grow even for well established alloys and new alloys—many with complex metallurgy-are being introduced. This series of reports has been developed to provide information regarding the most common boiler materials. Each report has been produced for an individual alloy; however, in order to gain a full appreciation for the metallurgical aspects of boiler steels, reference should also be made to the EPRI report Metallurgical Guidebook for Fossil Power Plant Boilers [1]. To facilitate the extraction of information, each volume in the series has been prepared using a similar format, with information presented on the following:

• Metallurgy covering microstructure and properties

• Standards and codes

• Fabrication issues

In each section, information of benefit to utility engineers is presented in a concise manner and supported by appropriate references to source documentation.

Arc welding is the most commonly used fabrication process employed for joining of HSLA Steel in normal varied section size in normal as well as in critical applications. The welding of high strength low alloy steels largely dominates their use in fabrication of various components of modern applications starting from manufacturing of automobile vehicles dealing with sheet metal to heavy engineering employs thick sections. According to their chemical composition these steel maintain good weldability due to low carbon and alloying contents. However, because of its comparatively complex weld thermal behaviour the multi-pass welding of thick sections of HSLA steels become critical in order to satisfy desired joint properties.

At high temperature exposure the interaction between metal or an alloy and the surrounding gases and combustion products leads to corrosion, thus leading to failure for materials and structures [2]. It is commonly reported that as a result of the oxidation process under isothermal conditions a protective Cr-containing oxide and Fe-containing oxide is developed on the surface of the steel causing a decrease of the oxidation rate with time. Oxide scale is constituted by a layered structure with compositional and microstructural variations from the substrate to the outer interface. On the other hand, depending on oxidation temperature and the chemical composition of the steel, both, the mechanisms of formation and the micro structural characteristics of the oxide scale, along with the degree of protection it provides are different.

All boilers and pressure vessels, regardless of their plate thickness, require mandatory post weld heat treatment (PWHT) as specified in Australian Standard for Pressure Vessel Manufacture [9].The main role PWHT is to relieve residual stress by allowing plastic flow at the stress relieving temperature as a result of decrease in yield strength.

In the present work effect of welding parameters on mechanical properties of SMAW welded Cr-Mo alloy steel and Hot Corrosion behaviour were studied.

The principal aim of the research was to establish the welding parameter to achieve desirable weldment properties and also study the oxidation behaviour of Cr-Mo boiler steel in Air atmosphere under isothermal conditions in cyclic manner.

LITERATURE REVIEW

2.1 Problem formulation Statement

To improve mechanical properties in pressure vessels and boiler steels considerable research efforts have been directed and many papers have described the methods of improving mechanical properties by conducting tests and results.

Nawrocki et al. [4] has worked on the tempering behaviour of simulated coarse-grained heat affected zone in alloy steel of 2.25Cr-1Mo steel which are used in power generation industry because of their elevated temperature strength and good creep resistance. The tempering behaviour of CGHAZ is done because this is typically the region of a weldment most susceptible to failure like reheat cracking, creep and hydrogen induced cracking.

They concluded that:

➢ The hardness decreased as time increased at temperature of 625°C and above.

➢ Microstructural study shows that steel experienced secondary hardening after tempering at 575°C for 5 hours; the secondary hardening is due to the Fe-rich M_3C carbides.

Klueh et al. [5] studied the effect of carbon on the microstructure, hardness, and the tensile properties of 2.25 Cr-1 MO steel with 0.009, 0.030, 0.120, and 0.135 wt % C. As annealed, the microstructure was primarily proeutectoid ferrite with spherical carbides and pearlite, the amounts increasing with increasing carbon content.
Conclusions were:

➢ During normalization (7/8 in rods or 1 in plates were heat-treated), granular bainite formed: 1 to 2 and 15 to 20% bainite (remainder proeutectoid ferrite) for the 0.009 and 0.030 wt % C steels, respectively; the 0.120 and 0.135 wt % C steels were entirely bainite.

> On tempering, carbides precipitated. In all heat-treated conditions, there was little difference in the room temperature hardness of the 0.009 and 0.030 wt % C steels and between the 0.120 and 0.135 wt % C steels.

> Tensile tests from 25 to 565°C indicated that strength depends on microstructure, which is determined by carbon cont

Shiue et al. [6] studied the influence of tempering treatments on toughness and austenite stability was conducted on modified 9Cr–1Mo welds. Deteriorated impact toughness was noticed for the welds tempered between 450 and 610°C for 1 h, in which the peak hardness and the lowest impact energy occurred at 540°C. The impact toughness of the welds increased rapidly at tempering temperatures above 680°C, and the associated fracture surface exhibited mainly dimple fractures for 750°C: 1 h tempered welds, in contrast to quasi-cleavage for 540°C:1 h welds. Retained austenite at martensite interlath boundaries was found to be mechanically stabilized by transformation stresses in the welds tempered at lower temperatures.

Conclusions were:

> The deteriorated impact toughness and a secondary hardening effect of modified 9Cr–1Mo welds tempered between 450 and 610°C:1 h were observed, in which the 540°C:1 h tempered specimen had the highest hardness and the lowest impact energy among various specimens.

> The existence of untempered martensite at interlath boundaries would contribute to the lowest impact toughness of the weld tempered at 540°C:1 h and deteriorate the already inferior toughness of the welds in the tempering range of 540–610°C for 1 h.

Sreenivasan et al. [7] presented Charpy energy (CV)–lateral expansion (LE) relations. In this note, after presenting the data for various steels in a single plot to get a global picture and discussing the dependence of the CV–LE plot on the type of steel, the data for particular classes of steels (austenitic stainless steels (SSs), AISI 403 martensitic SS, A533B steel, 9Cr–1Mo steels, etc.) are replotted in individual plots, and the mean quadratic fit to the plot is given as well as (where appropriate) the 95% confidence lower bound curve.

Conclusions were:

> Charpy energy (CV)–lateral expansion (LE) relations are useful in situations where a facility for measurement of LE is not available.

> Finally, CV normalized by yield stress has been shown to bring all the data into a single band and mean fit and 95% lower-bound curve equations have been derived and shown to predict LE from CV with acceptable conservatism for engineering purposes.

Dhooge et al. [8] studied the most recent information on the topic of reheat cracking in low alloys constructional steels, ferritic creep resisting steels, nickel-base alloys and austenitic stainless steels. Attention is paid to reheat cracking in weld metal, underbead cracking, the mechanism of reheat cracking and test methods.

Conclusions were:

> Weld metal reheat cracking has been reported to be related mostly to 2.25Cr-1Mo weldments, in which copper especially has a deleterious effect.

> To avoid this, stringent control of the Cu content in the weld metal and the use of non-Cu-coated wires for submerged arc welding are advised, together with welding techniques resulting in a maximum of grain refinement.

Chen et al. [9] studied the fatigue properties of ASTM A709 high performance steel. Because of its superior toughness, strength and weldability, high performance steel (HPS) has gained increasing popularity for use in highway bridges. Its fatigue resistance, however, is not yet well characterized. To study the fatigue behaviour of HPS, an analytical method that can predict both fatigue crack initiation and propagation is desirable.

Conclusions were:

> The HPS shows similar upper shelf energy absorption as A7 steel, but has a transition temperature 60°C lower than that of A7 steel.

> The HPS tested provides a significantly higher fatigue limit than conventional structural steels based on smooth specimen fatigue tests.

> The fatigue life prediction methods investigated in this research were found to predict fatigue test results very well. These methods provide a useful tool to derive fatigue curves for common details made of HPS.

Makhlouf et al. [10] studied the Fatigue crack growth behaviour of a duplex stainless steel in air environment at room temperature and in artificial sea water heated to 70 °C. Growth rates generated under constant load amplitude at a frequency of 0.1 Hz under corrosion fatigue were found to be about 1.7 orders of magnitude higher than those generated in air environment. The study of the crack propagation under both conditions has revealed a significant change in fracture mechanisms between both environments. The cyclic cleavage is induced by hydrogen embrittlement of the ferrite which is produced by an electrochemical reaction between the material and sea water.

Conclusions were:

> Growth rates in artificial sea water were found to be about 1.8 orders of magnitude higher than those generated in air environment.

> The fracture surface obtained by fatigue in air is predominantly transgranular and is composed basically of ductile fatigue striations on both phases and at all levels of _K.

> In artificial sea water, the crack proceeded by ductile fatigue striations only in austenite, whereas, it produced cleavage fracture in the ferrite .

Choi et al. [11] evaluated the integrity of socket weld in nuclear piping under the fatigue loading and deflection due to vibration. The pressure transient ranging from P = 0 to 15.51MPa and thermal transient ranging from T=250^{0}C to 2880^{0}C are applied.

Usman et al. [12] analysed the failure of T11 heat exchanger tubes used in ammonia plant which subjected to thermal fatigue from 850^{0}C to room temperature (250^{0}C). They also conducted experiments to confirm the site failure results. The experimental result shows close resemblance with the site results.

Brown [13] developed a hybrid method to analyse the creep-fatigue life of boiler components. The developed method provides sufficient conservatism while still maintaining economically designed components for combined cycle gas fired stations subjected to rapid start up and cooling transients. The work also suggests the use of the finite element method for thermal and stress analysis aids in the correlation between operational events and damage mechanisms.

King et al. [14] discussed about their recent experience in the condition assessment of boiler header components used in fossil fired power plants. The work faces many hurdles, which includes internal bore hole and ligament cracking and external tube connector weld cracking during operation. The work concluded that the failure of headers are due to the material degradation resulting from creep, high temperature headers can also experience thermal and mechanical fatigue.

Paterson et al. [15] presented a number of practical examples where component life monitoring has been implemented on power plants particularly in high temperature boiler headers and turbines. Headers are subjected to the damage mechanisms of creep due to on temperatures and pressures. Fatigue failures are due to start-up and shut-down where thermal transient occur. They developed a damage monitoring system to give substantial benefits to operators in terms of damage reduction and quantitative life assessment.

Tokiyoshi et al. [16] carried out thermal fatigue test on perforated plate. The applicability of the plate to the creep fatigue crack propagation life prediction is examined under high pressure and high thermal stress during plant operations. Inelastic analysis of perforated plate under thermal fatigue are carried out using finite element method (FEM) and compared with experimental results.

Kerezsi et al. [17] developed a test method for analysing the initiation and growth of cracks in pressure vessels and piping equipment. This method simulates the repeated thermal shock conditions produced in operating thermal power station equipment. The work suggested that the primary stress has little or no effect on crack initiation lifetime during repeated thermal shock below the creep range and the environmental interaction is highly influential in the growth of thermal shock cracks. The work also compared the experimental results with prediction methods from the ASME Boiler and Pressure Vessel Code.

Erwin et al. [18] analysed the failure caused of 101-C ammonia plant heat exchanger tubes. They suggested the failures are due to the formation and growth of internal oxide scales or deposits at areas of high heat flux. They presented a case history involving this type of failure. They analysed the failures using finite element modelling and recommended some methods to prevent this type of failure.

7

Wang et al. [19] investigated the behaviour of multiple stress corrosion cracks for two different metal environment combinations has emphasised the uncertainties associated with the development of individual cracks, concerning whether cracks arrest or grow and what growth rate is relevant.

Conclusions were:

> Multiple stress corrosion cracks occurred both in a Mn-Cr steel exposed to deionised water and Ni-Cr-MO-V steel exposed to 10M NaOH.

> Individual cracks exhibited stochastic features in their growth, with cessation of growth at certain stages and a wide range of velocities involved when growth occurred.

> Evidence is presented that coalescence of adjacent stress corrosion cracks in both systems can have a remarkable influence on the overall growth of cracks.

Hiromoto et al. [20] studied the Corrosion behaviour and microstructure of developed low-Ni Co–29Cr–(6, 8) Mo (mass %) alloys. The forging ratios of the Co–29Cr–6Mo alloy were 50% and 88% and that of the Co–29Cr–8Mo alloy was 88.The passive current densities of the low-Ni alloys were of the same order of magnitude as that of the ASTM alloy in all the solutions. The passive current densities of all the alloys did not significantly change with the inorganic ions and the biomolecules. Consequently, the low-Ni alloys are expected to show as high corrosion resistance as the ASTM alloy. On the other hand, the passive current density of the Co–29Cr–6Mo alloy with a forging ratio of 50% was slightly lower than that with a forging ratio of 88% in the saline. The refining of grains by further forging causes the increase in the passive current density of the low-Ni alloy.

He concluded that:

> Ni content in the air-formed surface oxide films of the low-Ni alloys and the ASTM alloys are under the detection limit of XPS and the surface compositions of the low-Ni alloys are similar to that of the ASTM alloy.

> The passive current densities of the low-Ni alloys are slightly higher than that of the ASTM alloy in saline solution

> The increase in grain boundaries by forging causes the decrease in corrosion resistance of the forged low- Ni alloy.

Wang et al. [19] investigated the behaviour of multiple stress corrosion cracks for two different metal environment combinations has emphasised the uncertainties associated with the development of individual cracks, concerning whether cracks arrest or grow and what growth rate is relevant.

Conclusions were:

➤ Multiple stress corrosion cracks occurred both in a Mn-Cr steel exposed to deionised water and Ni-Cr-MO-V steel exposed to 10M NaOH.

➤ Individual cracks exhibited stochastic features in their growth, with cessation of growth at certain stages and a wide range of velocities involved when growth occurred.

➤ Evidence is presented that coalescence of adjacent stress corrosion cracks in both systems can have a remarkable influence on the overall growth of cracks.

Hiromoto et al. [20] studied the Corrosion behaviour and microstructure of developed low-Ni Co–29Cr–(6, 8) Mo (mass %) alloys. The forging ratios of the Co–29Cr–6Mo alloy were 50% and 88% and that of the Co–29Cr–8Mo alloy was 88.The passive current densities of the low-Ni alloys were of the same order of magnitude as that of the ASTM alloy in all the solutions. The passive current densities of all the alloys did not significantly change with the inorganic ions and the biomolecules. Consequently, the low-Ni alloys are expected to show as high corrosion resistance as the ASTM alloy. On the other hand, the passive current density of the Co–29Cr–6Mo alloy with a forging ratio of 50% was slightly lower than that with a forging ratio of 88% in the saline. The refining of grains by further forging causes the increase in the passive current density of the low-Ni alloy.

He concluded that:

➤ Ni content in the air-formed surface oxide films of the low-Ni alloys and the ASTM alloys are under the detection limit of XPS and the surface compositions of the low-Ni alloys are similar to that of the ASTM alloy.

➤ The passive current densities of the low-Ni alloys are slightly higher than that of the ASTM alloy in saline solution

➤ The increase in grain boundaries by forging causes the decrease in corrosion resistance of the forged low- Ni alloy.

8

Raman et al. [21] studied the high temperature corrosion of chromium-molybdenum steel weldments to new vistas of life assessment of high temperature components by scale thickness measurement. Also, results are presented of a study to investigate the combined roles of the nature of the oxidising environment and of secondary precipitation on the extent of void formation in the weldments of chromium-molybdenum steel. Samples of microstructurally different regions, viz., weld metal, heat affected zone (HAZ) and base metal, were separated from the weldments of 2.25Cr-1Mo steel and oxidised in environments of steam and air. The resulting oxide scales and the region immediately beneath were characterised systematically using surface analytical techniques induced void formation were found to occur during steam oxidation, with a much greater intensity in the case of the HAZ sample.

They concluded that:

> Greater scaling rate of HAZ than weld and base metal regions of a 2.25Cr-1Mo steel weldment needs to be taken into account while using scale thickness measurement as a tool for life assessment of high temperature welded components.

> Given a suitable environment, a combination of chromium- rich secondary precipitation and extensive internal precipitation in the HAZ can result in further degradation of alloy microstructure which can facilitate crack propagation.

Andijani et al. [22] studied on the failure of boiler tubes by S- and V- induced hot corrosion.The phenomenon is usually noted on fire side of boiler tubes. Due to presence of sulfur in the combustion gases at high temperature, Ni, Cr, Fe or Al present in the boiler tube material undergo sulfidation which resulted in the formation of sulfide/sulfate. Vanadium compounds present in the combustion gases undergo fluxing reaction with oxide and/or sulphate scales on metal causing accelerated corrosion. The accelerated corrosion can cause pitting, cracking, fissure or rupture of the tubes. In this paper, the failure of some boiler tubes brought about mainly by S- and V induced hot corrosion will be described. An account of the possible mechanism(s) and the ways to combat such a type of corrosion is presented.

Conclusions:

> Failure of boiler tubes was due to localized overheating and subsequent dissolution of protective Al_2O_3 in the molten vanadium compounds followed by fluxing reaction resulting in the accelerated corrosion attack on the tube material.

> Failure of the tubes is most likely due to fuel ash corrosion. Presence of V and S in the tube surface deposits had accelerated the corrosion leading to perforation of the tubes. Use of Cr - containing steel SA 213-T22 (K21590) was recommended to minimize corrosion.

Pardo et al. [23] studied the pitting corrosion behaviour of austenitic stainless steels. Mn and Mo were introduced in AISI 304 and 316 stainless steel composition to modify their pitting corrosion resistance in chloride-containing media. Corrosion behaviour was investigated using gravimetric tests in 6 wt.% $FeCl_3$, as well as potentiodynamic and potentiostatic polarization measurements in 3.5 wt.% NaCl. Additionally, the mechanism of the corrosion attack developed on the material surface was analysed by scanning electron microscopy (SEM), X-ray mapping and energy dispersive X-ray (EDX) analysis.

He concluded that:

> Mn additions (from 0.3 to 1.7 wt %) have a detrimental effect on the pitting corrosion resistance of stainless steels studied in 3.5 wt % NaCl.

> Mn presence favours the formation of MnS inclusions with low electrochemical stability, which tends to dissolve, initiating an attack at the inclusion/matrix interfaces and being the initial step before a further pit propagation.

> Mo has effect on more than one step in a pitting event. In first instance, Mo modifies the passive film rendering it more stable against breakdown caused by the attack of aggressive Cl- ions.

Smith et al. [24] studied on The effect of a long post weld heat treatment on the microstructure and mechanical properties of a welded joint in a 0.2%C-1.4%Mn-O.S%Mo pressure vessel steel. Multipass submerged-arc welds were made at a heat input of 1.2 and 4.3 kJ mm^{-1}. Individual microstructural regions observed in the heat-affected zone of the actual weld were simulated. These regions were brittle in the as-simulated condition. Post weld heat treatment for periods of up to 40 h at 620 "C resulted in a significant improvement in the Charpy impact toughness.

Conclusions:

> The coarse grained heat-affected zone, subcrititally and intercritically reheated coarse grained heat-affected zone and intercritical heat-affected zone regions in the as-

welded (as-simulated) condition were brittle. Post weld heat treatment at 620°C resulted in a significant increase in toughness of these regions.

➤ Welding at a higher heat input results in a decrease in the heat-affected zone toughness compared to that of the low heat input welds. This is attributed to the presence of upper bainite in the coarse grained heat-affected zone. General decrease in the strength of the weldments. The strength still meets the minimum specified limits. No deterioration in toughness did occur. High weld metal toughness.

Swindeman et al. [25] studied on the operation of 9Cr–1Mo–V steel components in power boilers. Typical issues include chemistry effects, fabricability, weldability, fireside corrosion, steam side corrosion, aging, long-time creep, and damage accumulation.

Conclusions:

➤ The physical properties and strength of the Grade 91 give advantages over the Cr–Mo and 300 series stainless steels used for boiler construction in the USA, but there are issues that must be addressed in the use of the material.

➤ Of importance, is the welding technology with particular attention paid to filler metal chemistry and PWHT. Also, it should be recognized that the alloy will undergo significant aging effects during high temperature service that results in a lowering of both short time and long time strength.

➤ Efforts are underway on an international scale to better understand the degradation mechanisms in Grade 91 and other advanced Cr–Mo–V and Cr–W–V steels.

2.2 Introduction to High Temperature Corrosion

Many very important engineering systems operating at high temperatures (650°C-110°C) involve contact of metallic or ceramic materials with combustion product gases or other oxidizing gases containing inorganic impurities, e.g. gas turbines, steam generators, incinerators, and numerous petrochemical process vessels. As the gases are cooled, fused salt films may condense on the hardware to generate a highly corrosive condition analogous in some aspects to aqueous atmospheric corrosion.

Degradation by high temperature oxidation, hot corrosion and erosion are the main failure modes of components in the hot sections of gas turbines, boilers, industrial waste incinerators, metallurgical furnaces, petrochemical installations, etc. Super alloys have been developed for high temperature applications, but they are not able to meet the requirements of

both the high temperature strength and the high temperature erosion corrosion resistance simultaneously. One possible way to overcome these problems is the use of thin high temperature erosion corrosion and wear resistant coatings.

Aslasnar et al. [26] studied the effect of welding current on the quality of weld joint and obviously on tensile-shear and tensile-peel strengths of galvanized chromate steel sheets having 1.2 mm thickness in electrical resistance spot welding was investigated. A timer and current controlled electrical resistance spot welding machine having 120 kVA capacity and pneumatic application mechanism with a single lever was used to prepare the specimens. Welding periods were chosen as 5, 10, 12 and 15 cycles and also welding currents were increased from 4 kA up to 12 kA by rise of 1 kA. The electrode force was kept constant at 6 kN. The prepared welding specimens were exposed to tensile-shear and tensile-peel tests and the obtained results were supported by diagrams and, finally, appropriate welding parameters were advised to the users.

Sidhu et al. [27] studied on the behaviour of metals and alloys at elevated temperatures, especially their corrosion behaviour and providing protective surface layers has become an object of scientific investigation since long. No alloy is immune to hot corrosion attack indefinitely, although there are some alloy compositions that require a long initiation time at which the hot corrosion process moves from the initiation stage to the propagation stage. Nickel-based coatings have been reported to be widely used as they combine several advantages such as abrasion, erosion and resistance to high-temperature corrosive atmospheres. In this article, a brief review of the performance of nickel-based coatings has been made to understand their hot corrosion mechanism.

Conclusions:

> Hot corrosion is a serious problem in power generation equipment, gas turbines for ships and aircraft, and in other energy conversion and chemical process systems.

> Nickel based coatings such as Ni–Cr, Ni3Al, NiCrBSi and NiCrAlY have been found to exhibit excellent hot corrosion resistance.

> The formation of oxides and spinels of nickel, aluminium and chromium contributed to the development of hot corrosion resistance of these coatings.

Rathnamma et al. [28] studied hot corrosion in the hot gas pathways of marine gas turbines burning vanadium contaminated liquid fuels are presented here. A life prediction model, Life, is developed for turbine blades and guide vanes based on the application of fundamental heat, mass, and momentum transfer principles to the chemically reactive non-isothermal combustion environment. The corrosion rate is assumed to be limited by high Schmidt number diffusional dissolution of a protective oxide species into the condensed molten salt solution (equilibrium composition is predicted by means of free energy minimization by the computer program).

They concluded that:

> At sufficiently low surface temperatures, the solution deposition rate is insensitive to surface temperature.

> Molten salt deposition rate increases with an increasing fuel-to-air ratio, increasing gas main stream temperature, and with increasing sodium/vanadium concentrations in the combustion mixture. Relatively insignificant effects on the computed deposition rate.

Smith et al. [29] simulated a laboratory procedure for reproducing high temperature cracks found in coal fired boiler tubes. They proposed that the crack initiation is by an intergranular surface corrosion / thermal stress interaction mechanism and environmentally assisted thermal fatigue crack propagation.

Shiblia et al. [30] discussed about the new high strength martensitic steel P91 issues and compare some of the perceived benefits with the actual plant experience under creep – thermal fatigue conditions. They suggested that the use of the T91 or other 9Cr martensitic steel tubing is not recommended due to their high level of steam side oxidation and other related oxide characteristics.

Panda et al. [31] studied the corrosion behaviour of novel high carbon rail steels in simulated cyclic wet–dry salt fog conditions. Four new rail steels with microalloying elements, Cu, Cr, Ni and Si were designed. Quantitative evaluation done by weight loss measurements after simulated wet– dry salt fog exposure test showed similar weight loss values for all rail steels. Relative amounts of the different rust phases have been compared. SEM micrographs of the rusted samples revealed that the rust on Cr–Cu–Ni and Cr–Cu–Ni–

Si rail steel was more compact than other rail steels. Impedance spectroscopy showed that the rust formed on Cr–Cu–Ni and Cr–Cu–Ni–Si rail steels resulted in the higher impedance in the high frequency region, compared to other rail steels.

They concluded that:

➢ The corrosion behaviour of novel rail steels with Cu, Mo, Cr, Ni and Si alloying additions was studied by weight loss measurements.

➢ Weight loss values were similar for all the rail steels.

➢ SEM micrographs revealed that the rust on Cr–Cu–Ni and Cr–Cu–Ni–Si rail steel was more compact than other rail steels.

From the above literatures it is clearly found that thermal fatigue is an important phenomenon for the development of crack in pressure vessel components especially in super heater tubes. Many works was already done in studying the influence of thermal fatigue on failure of boiler headers using FEM. For simulating the thermal fatigue behaviour using laboratory setup is scarce with some constraints (dimensions and other conditions). In related to short–term overheating, failures are reported from the site and the cause for the failures are investigated in few works but simulating the short term over heating phenomenon is scare .

EFFECT OF HOT CORROSION IN BOILER STEELS AND TECHNICAL BACKGROUND OF Cr-Mo STEEL

3.1 Introduction to hot Corrosion

3.1.1 Definition of Corrosion:

Corrosion is defined as the destruction or deterioration of a material because of reaction with its environment [32]. Corrosion can be fast or slow depending upon its environment.

Corrosion can be classified in eight forms

1. Uniform Corrosion
2. Galvanic corrosion
3. Crevice Corrosion
4. Pitting Corrosion
5. Intergranular Corrosion
6. Erosion Corrosion
7. Stress- Corrosion
8. High temperature corrosion(Hot corrosion)

3.1.2 Hot corrosion

Hot corrosion is a high-temperature analogy of aqueous atmospheric corrosion. A thin film deposit of fused salt on an alloy surface in a hot oxidizing gas causes accelerated corrosion kinetics. Recognition of the problem and a search toward a mechanistic understanding and engineering abatement were initiated in response to the severe corrosion attack of military gas turbines during the Viet Nam conflict. Initially, the researchers were misled by the observation of corrosion product sulphides beneath a fused film of sodium sulphate to denote the problem and mechanism as "sulfidation". This fused salt (sodium sulphate) exhibited an acid-base character which at the time was quite uncertain and undefined. The electrolytic nature of the fused salt film and its similarity to atmospheric corrosion led to the more proper naming of the problem as "hot corrosion".

The operation of high temperature engineering systems, despite their associated material problems, is inherent to advanced technologies that strive to gain an advantage in

thermodynamic driving force or in reaction kinetics or both. Certain high temperature system involves the contact of materials with a large quantity, or significant depth, of a salt solution above its temperature. Such system include the molten carbonate fuel cell (MCFC), molten chloride baths to melt used aluminium beverage cans, the Hall-Heroult aluminium electrowinning cell with a fluoride(cryolite)-base electrolyte, nitrate/nitrite heat exange salts, fused salt descaling or heat treatment baths. In other important engineering systems, the accelerated corrosion of materials results from the contact of materials with thin films of deposited fused salts. This important corrosion made, analogous in certain aspects to aqueous atmospheric corrosion near room temperature, is called hot corrosion.

3.1.3 Effect of High Temperature Corrosion

Many very important engineering systems operating at high temperature (650-1100^{0}C) involve contact of metallic or ceramic materials with combustion product gases or other oxidizing gases containing inorganic impurities, e.g. gas turbines, steam generators, incinerators, and numerous petrochemical process vessels. As the gases are cooled, fused salt films may condense on the hardware to generate a highly corrosive condition analogous in some aspects to aqueous atmospheric corrosion.

Degradation by high temperature oxidation, hot corrosion and erosion are the main failure modes of components in the hot section of gas turbines, boilers, industrial waste incinerators, metallurgical furnaces, petrochemical installations, etc. Super alloys have been developed for high temperature applications, but they are not able to meet the requirement of both the high temperature strength and the high temperature erosion corrosion resistance simultaneously.

Khanna et al. [33] reported hot corrosion observed in boilers, diesel engines, mufflers of internal combustion engines and gas turbines. During the combustion stage in heat engines, particularly in gas turbines, sodium and sulphur impurities present either in or in combustion air, react to form sodium sulphate (Na$_2$SO$_4$). If the concentration exceeds the saturation vapour pressure at the operating metal temperature for turbine blades and vanes (700-1000^{0}C), then the deposition of Na$_2$SO$_4$ will occur on surface of this component s at high temperatures the deposits of Na$_2$SO$_4$ are molten (melting point-884^{0}C) and can cause accelerated attack of the Ni, Fe and Co-base super alloys.

According to Eliaz [34] et al Hot corrosion is divided into forms of attack:-

16

Type-1 high temperature hot Corrosion

Type-2 low temperature Hot Corrosion

Various parameters may affect the development of these two forms, including alloy composition and thermo mechanical condition, contaminant composition and flux rate, temperature and temperature cycles, gas composition and velocity and erosion process.

3.1.4 High Temperature (type-1) Hot Corrosion (HTHC)

Type-1 hot corrosion is observed mainly with the temperature range 850-950^{0}C when the salt deposit on the metal or alloy is in liquid state. Type-1 hot corrosion involves the transport of the sulphur from a sulphatic deposit (Generally Na_2SO_4) across a preformed oxide into the metallic material with the formation of the most suitable sulphides. The dominant salt in type -1 hot corrosion is Na_2SO_4 due to its high thermodynamic stability. Other impurities present either in the fuel or in the air, such as vanadium, phosphorous ,lead and chlorides, can combine with Na_2SO_4 to form compound with lower melting points. For example Na_2SO_4 (m.p. 884^{0}C) when combine with V_2O_5 (m.p. 670^{0}C), a eutectic is formed with a melting point of 550^{0}C, thus providing a aggressing environment. The macroscopy appearance of HTHC is characterised in many cases by severe peeling of the metal and by significant colour changes. For instance, greenish tonn appears on the surface of the metals and alloys due to formation of NiO in the area of accelerated attack. Microscopically the morphology of Type-1 is characterized by sulphidesed and depleted region beneath the porous, on protective scale.

3.1.5 Low Temperature (Type-2) hot corrosion (LTHC)

Type -2 Hot Corrosion usually occurs below melting point of Na_2SO_4. The reaction product morphology is characterized by a no uniform attack in the form pits, with only little sulphide formation close to the scale interface and little depletion of Cr or Al in the alloy substrate this form of Hot Corrosion is observed mainly with in the temperature range 650-800^{0}C the localised nature of attack is related to the localized failure of the scale as result of thermal cycling, erosion or chemical reactions. Microscopic sulphidation or chromium depletion is not generally observed in Type-2 hot corrosion.

Several metal and alloys react with air at elevated temperature, oxidation resistance must be considered in most of metallurgical application. As the temperature is increased, the

importance of metal oxidation is also increases as in the application of gas turbine, rocket engines, furnace at high temperature petrochemical system[32]. Given below is the cross section of the boiler where it is clear that boiler tubes are exposed to very high temperature.
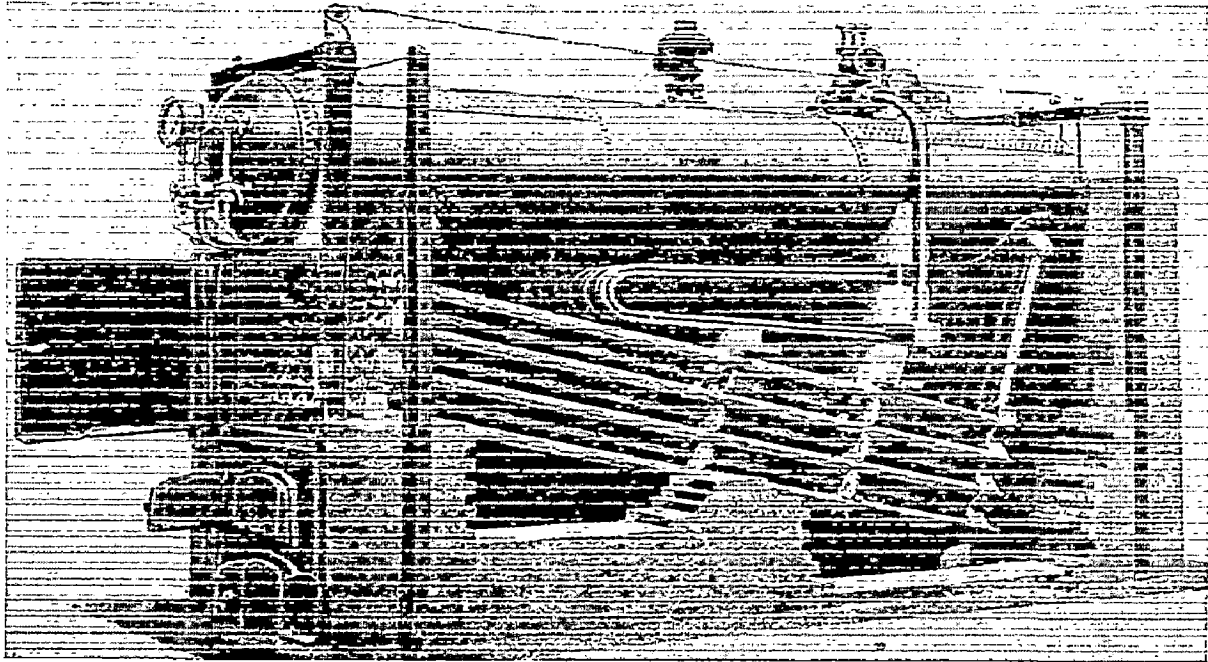
Fig. 3.1 Babcock and Wilcox boiler [34].

In water tube boiler, boiler feed water flows through the tubes and enters the boiler drum. The circulated water is heated by the combustion gases and converted into steam at the vapour space in the drum. These boilers are selected when the steam demand as well as steam pressure requirements are high as in the case of process cum power boiler/power boilers. Forced include and balanced draft provisions help to improve combustion efficiency.
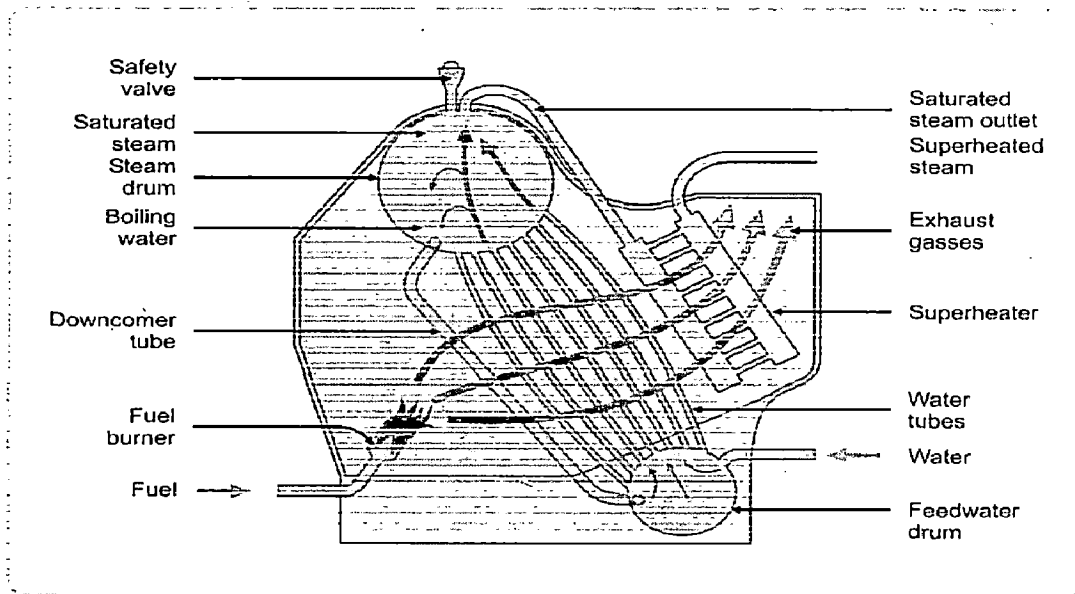
Fig. 3.2 Simple Diagram of Water Tube Boiler [35]

Most modern water boiler tube designs are within the capacity range 4,500-120,000 kg/hour of steam, at very high pressures. Many water tubes boilers nowadays are of packaged construction if oil and/ or gas are to be used as fuel. Solid fuel fired water tube designs are available but packaged designs are less common [35].

As seen above the tubes are directly coming in contact with flame thus leading to very high temperature of tubes and at this high temperature there is hot corrosion taking place.

3.2 Technical Background

Steels based on chromium (Cr) and molybdenum (Mo) are widely used in boilers and piping, and 1¼Cr½Mo (Grade 11) low alloy steels have been standardized in countries across the world for more than 50 years [3]. The Grade 11 is most commonly used in North America. Grade 11 alloys contain up to 1% silicon (Si) and are sometimes identified as 1¼Cr½MoSi. The high Si level in Grade 11 steel is added for better oxidation, scaling, and fireside corrosion resistance, which is particularly important in tubing. Example specification numbers from the United States (as specified by [ASTM]), UK and Japan are given in Table3.1.

Table 3.1 Examples of International Specifications for Grade 11 Steel

ASTM	British	Japanese
SA-213 T11	3606 S1 621	G 3462 STBA23

The alloys now widely known as *Grades 11* based on the ASTM alloy designations have been used successfully in power plant applications that require reasonable high-temperature strength (derived primarily from a dispersion of fine Mo carbide precipitates) and resistance to oxidation (derived from the Cr present). The most common applications are in superheater and reheater tubing as well as high-temperature headers and piping where operation up to about 1112°F (600°C) is required. In fact, different codes and manufacturers recommend different peak temperatures for Grade 11 steels. An example is shown in Table 3.2

Table3.2 Peak Temperatures Recommended by Code and Manufacturers

ASME Specification	ASME °F/°C	Babcock & Wilcox °F/°C	ALSTOM °F/°C	Riley °F/°C
SA-213 T11	1200/649	1050/566	1025/552	1025/552

Experience suggests that for excellent long-term performance, the sustained metal temperature should be below about 1050°F (566°C); however, it is apparent that the specific information regarding pressure, temperature, and environment should be considered when selecting material and component geometry.

3.3 Forms Available

Grade 11 alloys are available in the following forms:

• Tubes

• Pipes

• Forgings

• Castings

• Bars

• Rods

• Plates

• Sheets

3.4 Applications

Grade 11 alloys are used in the following applications:

• High-pressure boilers

• Superheaters

• Drying ovens

• Air preheaters

• Incinerators

• Heat exchangers

• Other high-temperature service where good creep strength or resistance to corrosion and oxidations or both is desired.

EXPERIMENTATION

Base material of Cr-Mo alloy steel of ASTM SA387 Gr-11 is selected for the project. Electrodes of E8018 B2 are selected which are low hydrogen electrodes. Electrodes are backed at 200 ^{0}C, base material is preheated at 200 ^{0}C in the furnace before use. Welding is done by choosing Double-v groove as joint design. Sectioning of the weldment is done as per the requirements for hardness, tensile, charpy impact test, microstructural study and corrosion testing. The specimens are prepared for testing hardness, tensile strength, charpy impact toughness, microstructural study.

4.1 Experimentation Details

4.1.1 Chemical Composition

The chemical compositions of Grade 11 steel specified by ASME SA-387 Gr-11 given in the ASTM's Handbook of Comparative World Steel Standards [36] are given in Table .The basic requirements have changed little since the introduction of these steels more than 50 years ago. However, improvements in steel making practice have allowed greater control of trace elements, such as phosphorus and sulphur.

Table 4.1 Composition of Grade 11 Low Alloy Steels According to ASME SA- 387 Gr-11:-

	ASTM SA 387 Gr-11
Carbon	0.05–0.15
Manganese	0.30–0.60
Silicon	0.50–1.00
Phosphorus	0.025 Maximum
Sulphur	0.025 Maximum
Chromium	1.00–1.50

Nickel	-
Molybdenum	0.44–0.65
Others	-

4.1.2 Physical Properties of Cr- Mo alloy steel

• The *elastic modulus* of a material represents the relative stiffness of the material within the elastic range and can be determined from a stress-strain curve by calculating the ratio of stress to strain. Values are normally determined from tests performed in tension. The modulus of elasticity diminishes from 215 gigapascals (GPa) (30 × 106 pounds per square inch [psi]) at room temperature to 140 GPa (20 × 106 psi) at 760°C (1400°F).

• *Modulus of rigidity*, also known as the *shear modulus*, is the coefficient of elasticity for a shearing force.

• The *coefficient of linear thermal expansion* is the ratio of the change in length per degree Kelvin (K) to the length at 273 K (32°F). If l_0 is the length at 273 K and alpha is the coefficient of linear thermal expansion, the length at temperature T, l_t, is given by

$$l_t = l_0(1 + \alpha T)$$

• The *thermal conductivity* (k) is the quantity of heat transmitted as the result of unit temperature gradient in unit time under steady conditions in a direction normal to a surface of unit area, when the heat transfer is dependent only on the temperature gradient.

• The *specific heat* (Cp) is the amount of heat measured in calories required to raise the temperature of one gram of a substance by 1°C (34°F). At room temperature, the value is 442 joules per kilogram (J/kg), with K increasing to 688 J/kg K at 527°C (981°F).

• The *specific gravity* is the ratio of the density of a substance to the density of water.

• *Poisson's ratio* is the lateral contraction per unit breadth divided by the longitudinal extension per unit length. Poisson's ratio increases from 0.288 at room temperature to 0.336 at 760°C (1400°F).

Thermal diffusivity is the constant in the heat conduction equation describing the rate at which heat is conducted through a material. It is linked to thermal conductivity, specific heat, and density (ρ).

Table 4.2 Typical Physical Properties at Room Temperature

	English Units	SI Units
Specific gravity	7.83	7.83
Density	0.2833 lb/in^3	7.83 g/cm^3
Thermal coefficient of expansion	7.3 x 10^{-6} °F (70–1000°F)	13.2 x 10^{-6} °C (21–538°C)
Modulus of elasticity at room temperature	29.7 psi x 106	215 GPa
Modulus of rigidity or shear modulus at room temperature	12.0 psi x 106	83 GPa
Specific heat	0.105 Btu/lb/°F (120–210°F)	442 J/kg K at 23°C 688 J/kg K at 527°C 969 J/kg K at 727°C
Thermal conductivity	23 (Btu.ft/ft2.hr/°F [70°F])	39.5 (W/m-°C [21°C])
Poisson's ratio at room temperature	0.288	0.288

Notes:

1 *Btu* stands for *British thermal unit(s)*.

2 *W* stands for *watt(s)*; *W/m* stands for *watt(s) per meter*.

4.1.3 Electrode configuration for sa-387 gr-11 steel E-8018-B2

E- Electrode

80- Min, Tensile Strength, Ksi

1-All position

8- Iron Powder, Low Hydrogen AC or DCEP (Electrode Positive)

B2- Chemical Composition of Weld Deposit.

AWS Class E8018-B2

AC-DCEP (Electrode Positive)

Electrodes of AWS class E 8018-B2 with 4 mm diameter are selected which are low hydrogen electrodes used commonly for pressure vessels, heat exchangers and boilers and high pressure pipe line etc. This electrode had been manufactured by D& H Secheron Company.

4.1.3.1 Typical mechanical properties

	Stress Relieved	
	1 hr.	8 hrs.
	@1275°F (691°C)	@1275°F (691°C)
Yield Strength, psi (MPa)	77,400 (534)	71,800 (495)
Tensile Strength, psi (MPa)	89,700 (618)	85,800 (592)
% Elongation in 2" (51 mm)	26	27
% Reduction of Area	70	71

4.1.3.2 Typical Undiluted Weld Metal Analysis (%)

C	Mn	Si	P	S	Cr	Mo
0.067	0.64	0.45	0.016	0.014	1.23	0.55
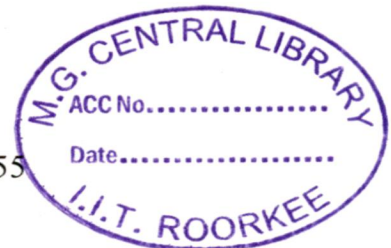
> Electrodes are backed at 250^0C before use for one hour in the furnace.
> Preheat should be used on hardenable steels to prevent the formation of a hard heat-affected zone at temperature of 200^0C – 300^0C.
> Preheat may also be required in welding heavy sections.

In all arc welding process it is necessary to closely match the weld metal deposited with the composition of the base metal. Filler metal of the same or slightly higher alloy content can be used for welding several Cr-Mo steels.

4.1.4 Welding parameters

Electrode	E8018-B2
Joint geometry	double V (60^0 included angle)
Type of current and polarity	DCEP
Preheating temperature	200^0C
Interpass temperature	200^0C
Electrode diameter for Root passes	4mm
Electrode diameter for filler passes	4mm
Welding Voltage	24V
Welding current	130-170A

4.1.5 Joint preparation

4.1.5.1 Open Butt Joint

When a complete pipe or fitting has to be replaced, some form of joint preparation will be required to ensure proper fit-up and to provide adequate access for welding. It is not always appropriate to duplicate the groove design used during original fabrication because the replacement has to be performed *in situ* where access might be difficult and there are equipment restrictions. It is essential to select a weld joint configuration that will provide reasonable access for achieving acceptable weld quality but which does not require an excessive amount of welding time. Selecting a weld groove angle that is too wide will require an unnecessary amount of welding time. Although the weld groove geometry is not an essential variable for the ASME Section IX WPSs that cover the commonly used GTAW and SMAW processes, it is recommended that standard weld joint preparations for butt welding be selected whenever possible. The important features of a weld preparation are the following:

• Included angle

• Root opening

• Root face

• Radius at the root

Figure 4.1 shows the various elements in a typical weld joint end preparation. Both the included angle of the groove and the root opening directly affect the access of the welding electrode. The proper combination is needed to avoid a lack of sidewall fusion defects, which result if the weld groove is too narrow. If the weld groove is too wide, it will result in unnecessary welding. The root opening and the root face are critical in ensuring good root fusion without melting through. A too-wide opening and too-thin root face will usually result in excessive penetration and/or melt-through. An opening that is too narrow and root face that is too thick will result in lack-of-penetration defects.
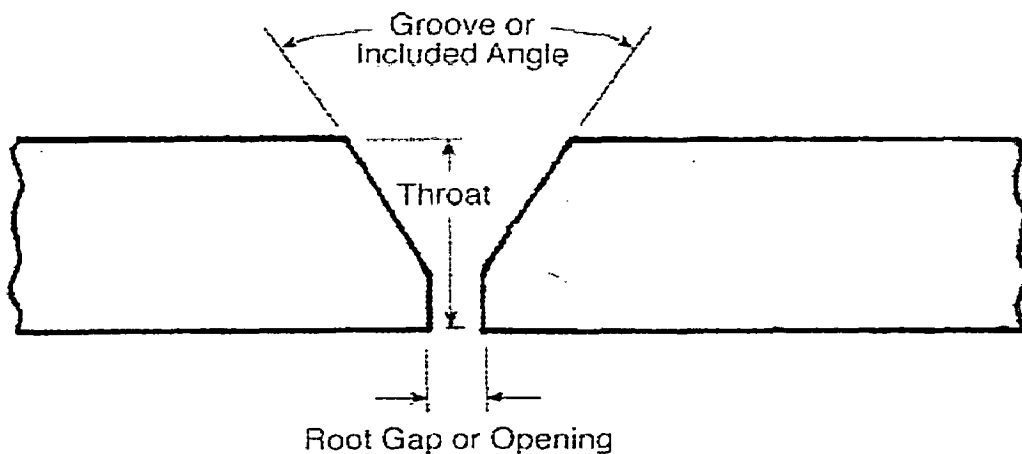
Figure 4.1 Groove Weld End Preparation Nomenclatures

4.1.6 Welding process selected

4.1.6.1 Shielded metal arc welding

A written welding procedure qualified in accordance with ASME Section IX is required for pressure boundary welding. The purpose of the procedure qualification is to ensure that the weldment exhibits the required properties for the intended application. The requirements needed to qualify a welding procedure for pressure boundary components are specified in ASME Section IX, "Welding and Brazing Qualifications." It is imperative that the correct welding procedure be chosen for the application. A welding procedure should consist of a WPS and a procedure qualification record (PQR). The WPS gives direction to the welders for making the production welds. Both essential and nonessential variables listed in ASME Section IX for the particular process employed should be included on the WPS. The PQR should list the essential variables used to weld the test coupons and the test results.

4.1.6.1.1 The Process

Shielded metal arc welding (SMAW) is a process that melts and joins metals by heating them with an arc established between a stick like covered electrode and the metals, as shown in Figure It is often called stick welding. The electrode holder is connected through a welding cable to one terminal of the power source and the work piece is connected through a second cable to the other terminal of the power source as shown in the Figure 4.2(a). The core of the covered electrode, the core wire, conducts the electric current to the arc and provides filler metal for the joint. For electrical contact, the top 1.5 cm of the core wire is bare and held by the electrode holder. The electrode holder is essentially a metal clamp with an electrically insulated outside shell for the welder to hold safely. The heat of the arc causes both the core wire and the flux covering at the electrode tip to melt off as droplets Figure 4.2(b). The molten metal collects in the weld pool and solidifies into the weld metal. The lighter molten flux, on the other hand, floats on the pool surface and solidifies into a slag layer at the top of the weld metal.
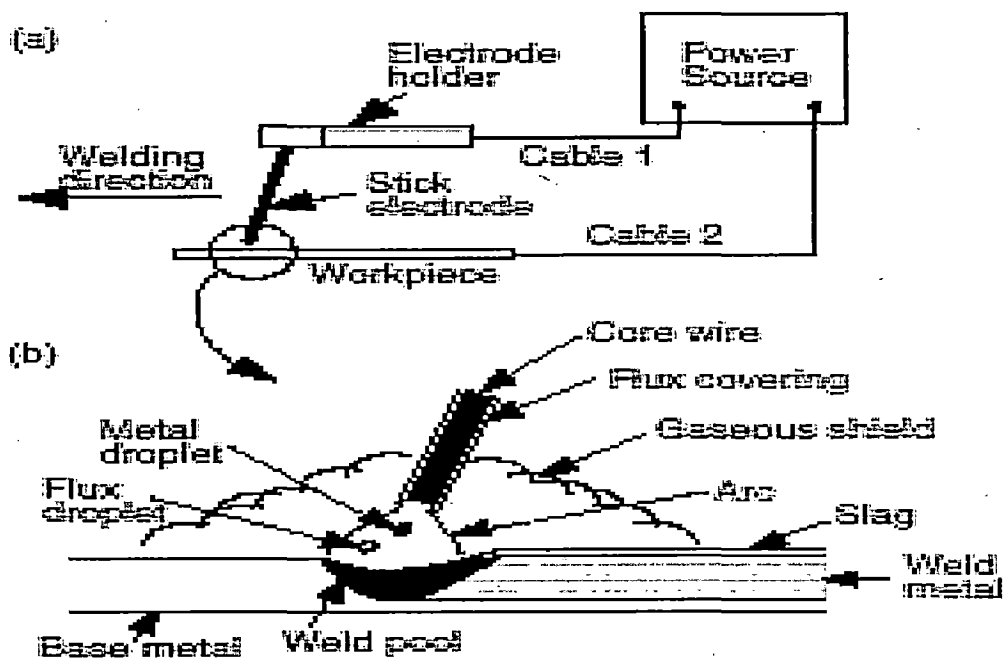

Figure 4.2 Shielded metal arc welding: (*a*) overall process; (*b*) welding area enlarged [30].

4.1.6.1.2 Functions of Electrode Covering

The covering of the electrode contains various chemicals and even metal powder in order to perform one or more of the functions described below.

A. **Protection:** It provides a gaseous shield to protect the molten metal from air. For a cellulose-type electrode, the covering contains cellulose, $(C_6H_{10}O_5)$ $_x$. A large volume of gas mixture of H_2, CO, H_2O, and CO_2 is produced when cellulose in the electrode covering is heated and decomposes. For a limestone- $(CaCO_3-)$ type electrode, on the other hand, CO_2 gas and CaO slag form when the limestone decomposes. The limestone-type electrode is a low-hydrogen type electrode because it produces a gaseous shield low in hydrogen. It is often used for welding metals that are susceptible to hydrogen cracking, such as high-strength steels.

B. **De-oxidation:** It provides deoxidizers and fluxing agents to deoxidize and cleanse the weld metal. The solid slag formed also protects the already solidified but still hot weld metal from oxidation.

C. **Arc Stabilization:** It provides arc stabilizers to help maintain a stable arc. The arc is ionic gas plasma) that conducts the electric current. Arc stabilizers are compounds that decompose readily into ions in the arc, such as potassium oxalate and lithium carbonate. They increase the electrical conductivity of the arc and help the arc conduct the electric current more smoothly.

D. **Metal Addition:** It provides alloying elements and/or metal powder to the weld pool. The former helps control the composition of the weld metal while the latter helps increase the deposition rate.

4.1.6.1.3 Polarity:

Figure 4.3 shows three different polarities, which are described next.

➢ **Direct-Current Electrode Negative (DCEN):** This, also called the straight polarity, is the most common polarity in SMAW. The electrode is connected to the negative terminal of the power supply. A significant amount of energy, called the work function, is required for an electron to be emitted from the electrode. When the electron enters the work piece, an amount of energy equivalent to the work function is released.
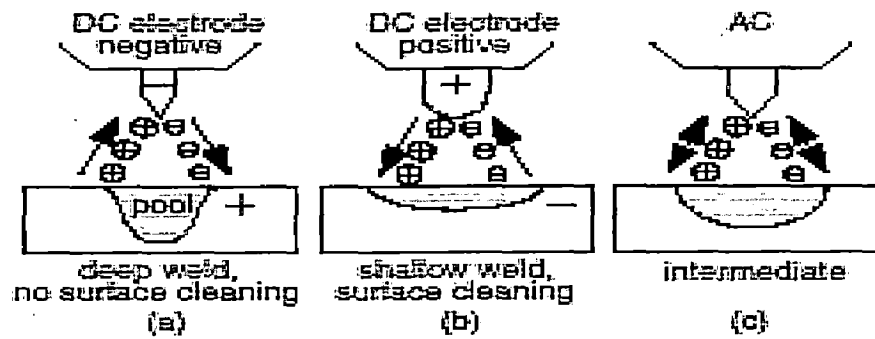
Figure 4.3 Three different polarities.

➤ **Direct-Current Electrode Positive (DCEP):** This is also called the reverse polarity. The electrode is connected to the positive terminal of the power source. As shown in Figure 3.2, the heating effect of electrons is now at the electrode rather than at the work piece. Consequently, a shallow weld is produced. Furthermore, large-diameter, water-cooled electrodes must be used in order to prevent the electrode tip from melting. Therefore, DCEP can be used for welding thin sheets of strong oxide-forming materials such as aluminium and magnesium, where deep penetration is not required.

➤ **Alternating Current (AC):** Reasonably good penetration and oxide cleaning action can both be obtained. This is often used for welding aluminium alloys.

4.1.6.1.4 Power supply:

The power supply used in SMAW has constant current output, ensuring that the current (and thus the heat) remains relatively constant, even if the arc distance and voltage change. This is important because most applications of SMAW are manual, requiring that an operator hold the torch. . Maintaining a suitably steady arc distance is difficult if a constant voltage power source is used instead, since it can cause dramatic heat variations and make welding more difficult.

4.1.6.1.5 Advantages and Disadvantages

The welding equipment is relatively simple, portable, and inexpensive as compared to other arc welding processes. For this reason, SMAW is often used for maintenance, repair, and field construction. However, the gas shield in SMAW is not clean enough for reactive metals such as aluminium and titanium. The deposition rate is limited by the fact that the

30

electrode covering tends to overheat and fall off when excessively high welding currents are used. The limited length of the electrode (about 35 cm) requires electrode changing, and this further reduces the overall production rate [33].

4.1.7 Process selection:

Because of its versatility and simplicity, it is particularly dominant in the maintenance and repair industry, and is heavily used in the construction of steel structures and in industrial fabrication. However, because of the low equipment cost and wide applicability, the process will likely remain popular, especially among small businesses where specialized welding processes are uneconomical and unnecessary. SMAW is used to weld carbon steel, low and high alloy steel, stainless steel, cast iron, and ductile iron. While less popular for nonferrous materials, it can be used on nickel and copper and their alloys and, in rare cases, on aluminium. Furthermore, depending on the electrode used and the skill of the welder, SMAW can be used in any position.

With such versatility in application SMAW can be used most suitably to assess weldability considerations in steels like Cr-Mo boiler grade steel with necessary precautions with the help of flaw detection and assessment through various NDT and DT techniques and hence SMAW is chosen as the desired welding process.

These alloy steels are air-hardening and subject to cracking if not properly handled. Because of the hardenability conferred by the alloying elements present. To weld these tubes, it is necessary to use low hydrogen coated electrodes. Thus, for shielded metal arc welding (SMAW), an E8018-B2 electrode is typically used. A 250°F (121°C) minimum preheat is appropriate for thick joints (t > ½ in.) with high restraint and a minimum specified tensile strength in excess of 60 ksi. Welds in thinner sections can be made without preheat, but exemption from PWHT is usually contingent on a minimum preheat of 250°F (121°C

4.1.8 Collection of specimens from Weld joints

Sectioning of the weld joints for fabrication of various test specimens was made with the help of band saw. The collection of specimens for mechanical testing, metallography and Hot Corrosion test from different locations of the weld joints has been schematically shown in Fig. 4.4.
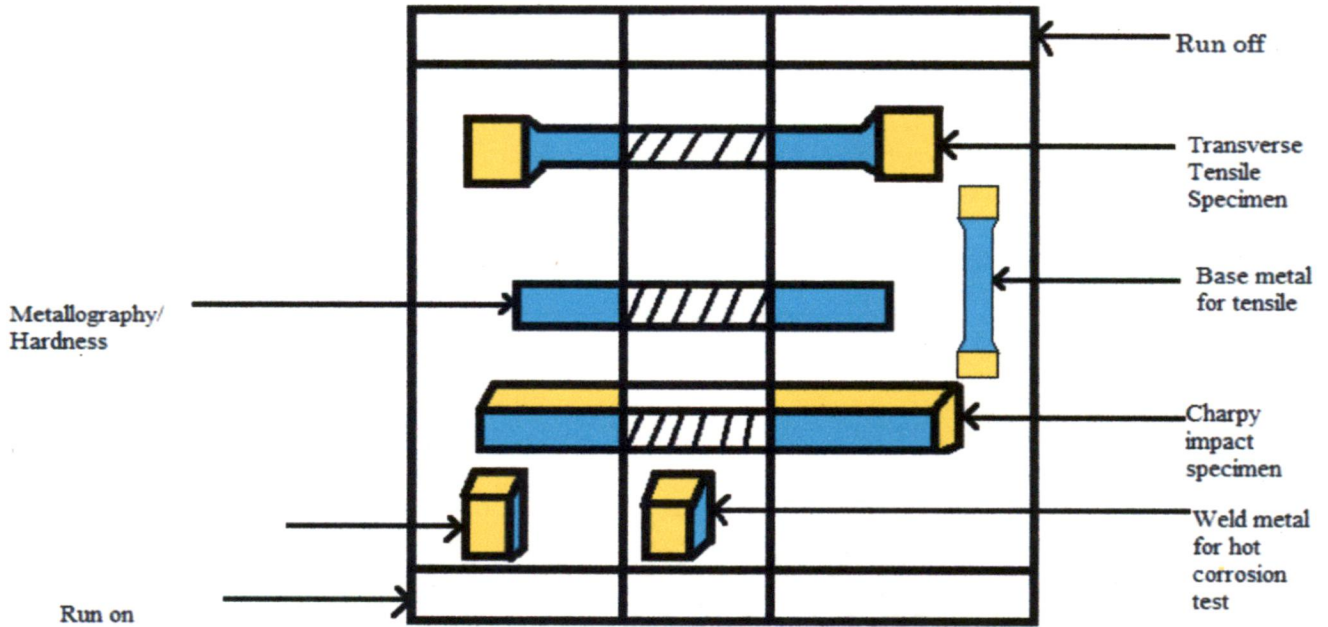
Fig 4.4: Collection of samples from weld joints.

4.1.9 Testing of mechanical properties

The weld joint are prepared using the SMAW process. After the collection of material was done as shown in above figure as per the required dimensions. The specimens for testing's are sectioned using band saw.

4.1.9.1 Tensile test

Tensile properties of the base metal and weld joint, with respect to their ultimate tensile strength(UTS), yield strength(YS), percentage area of reduction(%RA) and percentage elongation were studied by using round tensile test specimen as per ASTM E8M standard. Tensile properties of weld joint were studied by using weld for axial weld (weld at centre) the axial weld specimens are prepared by keeping the weld at centre of the gage length. The test is carried out on 6 tonn servo-hydraulic microprocessor controlled universal testing machine. The graph between stress and strain, yield strength, ultimate strength has been recorded. The percentage elongation in length and percentage reduction in area has been evaluated separately.

Dimensions of the specimen are:-

D-diameter-6±0.1mm

A- length of reduced section-24mm

G-gage length-30±0.1mm

R-radius of fillet-4mm
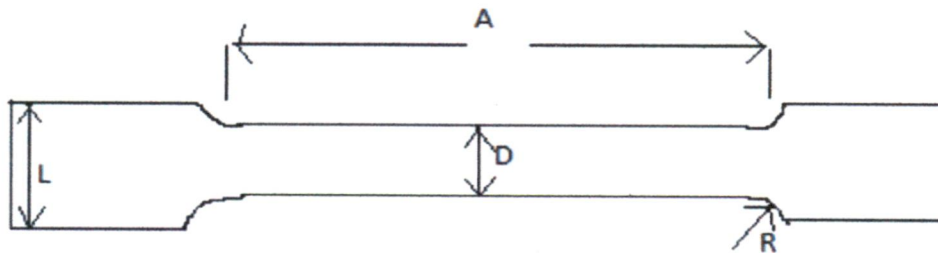
Fig4.5: Schematic diagram for tensile specimen

Fig4.6: Weld joints at different process parameter

Fig4.7: Tensile test specimens

Fig4.8: Tensile specimens after testing

4.1.9.2 Hardness Testing

Hardness test is conducted on the welded samples. Samples of 15mm width and 60mm length were cut from the welded material and are polished from measurement for hardness. Specimens having all the three portions of a weldment viz. Weld metal, HAZ and base metal was tested using micro-hardness tester. The hardness is taken from the centre line towards base metal.
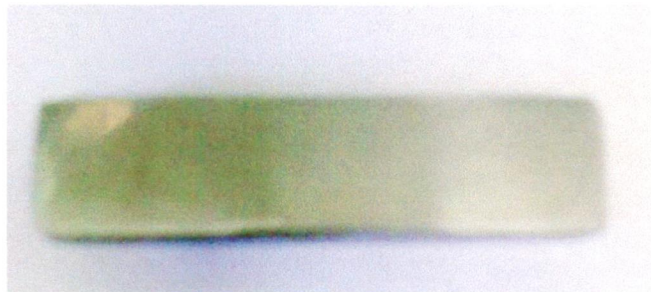
Fig 4.9: Sample for microhardness testing.
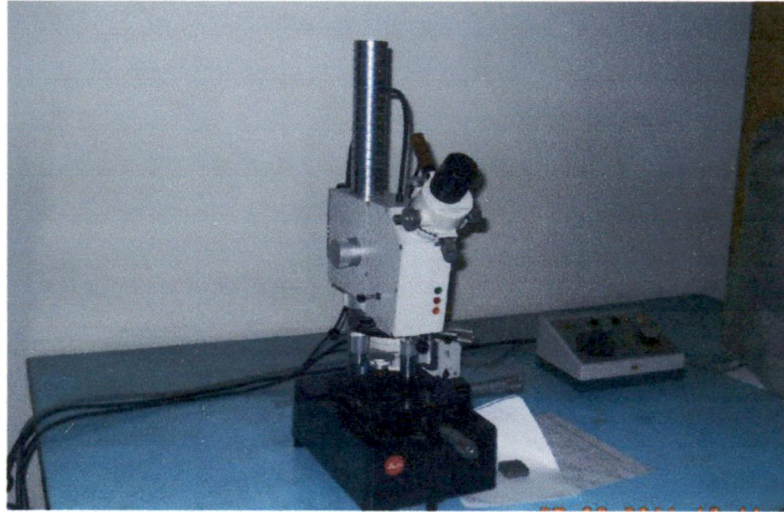
Fig 4.10: Microhardness testing machine

4.1.9.2.1 Parameters selected for hardness testing are:

Hardness type: Micro hardness

Load: 100gms=980mn

Dwell time; 30 seconds

The hardness measurements points are taken at a distance of 1mm in weld metal, base metal.

4.1.9.3 Charpy-V-notch Impact Specimen

The standard charpy V-notch specimen were taken in transverse manner. The notch was made in transverse direction at the weld centre, so that the cracking plane lies along the direction of welding.

The specifications of impact testing machine are:-

Pendulam velocity: 5.4 meter per second

Range: 0-300 joule

Least count: 2 joule

Specimen size: 55×10×10mm as per ASTM E-23 standard.
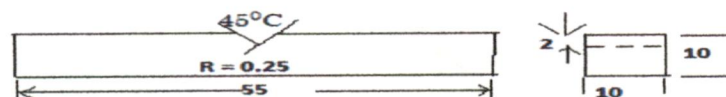
Fig4.11: Dimensions of charpy-V notch specimen[43].
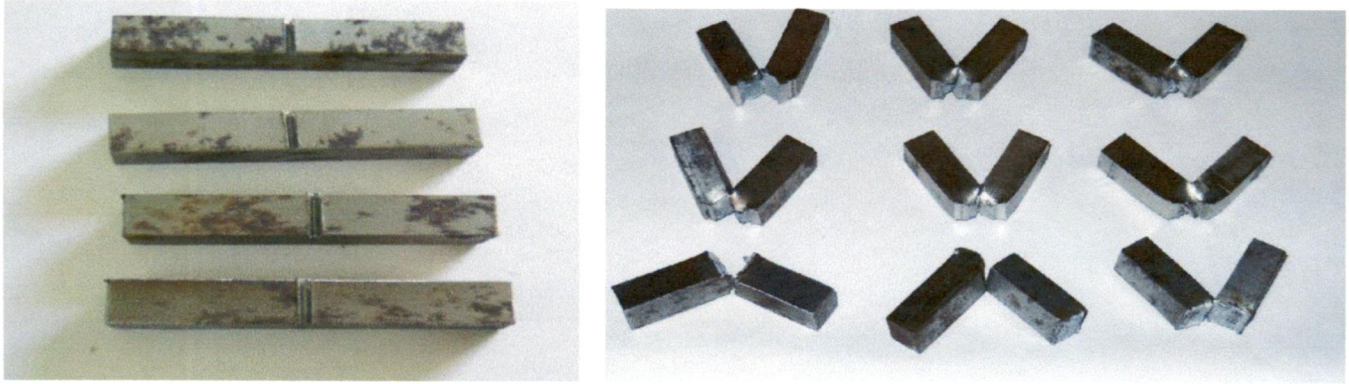
Fig 4.12: Specimens used for charpy test

4.1.9.4 Microstructural Examination

Microstructural examination is done on as welded conditions. Samples of 10mm width and 50mm length were cut tranverse to the weld for microscopic examination. The sample were polished and etched 10% Nital solution for 10-20 seconds in order to check the different location in weld metal ,HAZ and base metal.

Fig 4.13: Optical Microscope used for Micrographs

4.1.9.4.1 Sample preparation

1-Paper polishing

-220 Grit SiC paper

-400 Grit SiC paper

-600 Grit SiC paper

-1000 Grit SiC paper

-1100 Grit SiC paper

(This step may be repeated 2-3 times)

2- Cloth polishing:-

Soft cloth allows greatest shock absorbency and therefore allow for gentle polishing with little damage. Soft cloths allow the abrasives to abrade.

Soft cloth-

-a super scratch removal

- risk generating surface 'relief'

Using alumina (Aluminium oxide) Al_2O_3 as a paste on cotton cloth.

4.1.9.5 Etching:

Etching delineates the grain structure. Etching may attack a second attack a second phase preferentially or attack boundaries excessively. Caution should be taken when choosing and using etchants. Impact the sample surface using a light microscope before and after etching to asses' effect. Materials that are difficult to polish may benefit from repeated etching and polishing.

After preparing samples, microstructural study had been done using optical microscopy and scanning Electron Microscope (SEM) for getting microstructure of all processed samples. The microstructural study is focused on weld metal, HAZ and base metal.Breifly studied the microstructures at different magnification like 50x, 100x,250x.observed the microstructure changes taking place by the effect of PWHT in weld metal, HAZ and base metal.

4.2 Hot Corrosion study

Hot corrosion tests are conducted on 1%Cr-0.5%Mo alloy steel of ASTM SA387 Gr-11, which are commonly used as boiler tube material in super heater, reheater and other parts especially when the service conditions are stringent from point of temperature and pressure. These materials are also used in pressure vessels, piping in the chemical industry, baffle plates/tubes in the fertilizer plant. The material from CSC steel Navi Mumbai in the form of plate in rolled condition. The composition is mentioned in initial pages. The hot corrosion test was conducted on base metal and weld metal in order to study the corrosion effect on weld and unweld condition.

4.2.1 Preparation of specimens for testing

Specimens with dimensions are approximately were cut from the plates and polished using emery paper of 200, 400, 600, 800 and 1000 grit sizes and mirror polished using clothe polishing wheel machine with 1μm lavigated alumina powder suspension. The specimens were prepared manually and all care was taken to avoid any structural changes in the specimens.

4.2.2 Experimental procedure

After sample preparation, samples were placed on the ceramic boat. The experimental setup used for one has been shown in figure. Hot corrosion studies were conducted at 900^0C in laboratory silicon carbide tube furnace. The furnace was calibrated to an accuracy of $\pm5^0C$ using platinum-rhodium thermocouple fitted with a temperature indicator. The physical dimensions of the specimens were recorded carefully with sylvac digital vernier calliper to evaluate their surface areas.

The specimens were washed properly with acetone and dried in hot air to remove moisture. During experimentation, the prepared samples were kept in an alumina boat and the weight of boat and specimens was measured. The alumina boats used for the studies were preheated at a constant temperature of 120^0C for 3 hours, and it is assumed that their weight would remain constant during the course of high temperature corrosion study.

Cyclic oxidation studies were performed in air for 50 cycles, with each cycle consisting of 1 hr heating at 900^0C, followed by 20 min cooling at room temperature. The aim cyclic loading is to create severe boiler environment conditions for testing. The hot corrosion tests are conducted in air at 900^0C.

The boat containing the specimen was inserted in to hot zone of the furnace maintained at temperature of 900^0C. The weight of the boat loaded with the specimen was measured after each cycle during the corrosion test. Weight change measurements were taken at the end of each cycle using an electron balance (model 06120) with a sensitivity of 1mg. At the time of weighing, even the spalled scale was also included to determine the total rate of corrosion.

The Specimens were subjected to visual observations carefully after the end of each cycle with respect to colour, spalling and peeling of scale during cyclic corrosion. The above experiments were conducted for 50 cycles.
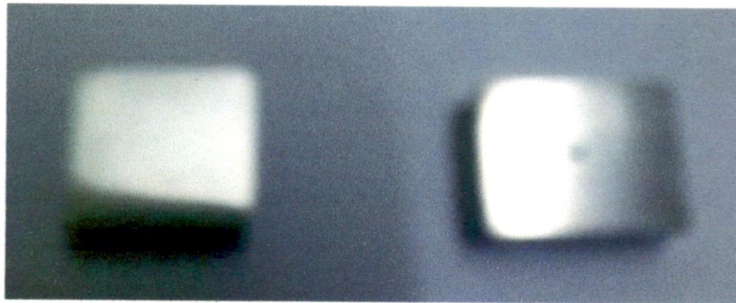
(a)

(b)

(c)
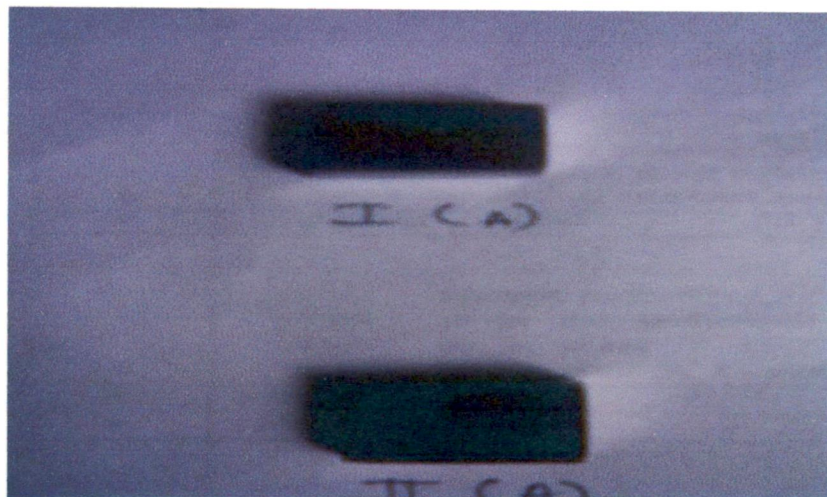
(d)

Fig.4.14 (a) BM and WM sample (b) Furnace (c) Sample placed in ceramic boat (d) After corrosion WM and BM

4.2.3 Analysis of Hot Corrosion test

All the specimens subjected to hot corrosion were analyzed for the characterization of corrosion products.

4.2.3.1 Visual observations

After every hot corrosion cycle surface was the specimens was visually examined for change in colour, luster, spalling tendency, and growth of cracks. The spalled scale was also included to determine the total rate of corrosion.

4.2.3.2 Weight change studies

The weight change values were measured at the end of each cycle with the aim to establish the kinetics of oxidation and hot corrosion. The weight change data was plotted with respect to number of cycles. The weight change is due to formation of the oxide scales, spalling and sputtering etc.

RESULTS AND DISCUSSIONS

5.1 Microstructure

The microstructures of the weld metal, HAZ and BM have been studied to find out the behaviour of the grain growth and its structure at different location along the weld joint. Micrographs have been taken at different magnifications with the help of optical microscope to ensure the better understanding of the microstructure.

In practical applications, slow cooling will often occur after heat treatment of large, thick section components, and in these components, largely ferritic microstructures are seen (see Figure 5.1). In most of these cases, the transformation product will be pearlite; however, at intermediate cooling rates, transformation to pearlite and bainite can occur. Lath martensite is formed in HAZ, which is having high hardness. Chances for formation of lath martensite are due to high carbon percentage and rapid cooling. The weld metal in as welded condition shows lath bainite with fine distribution carbides in the ferrite grains.
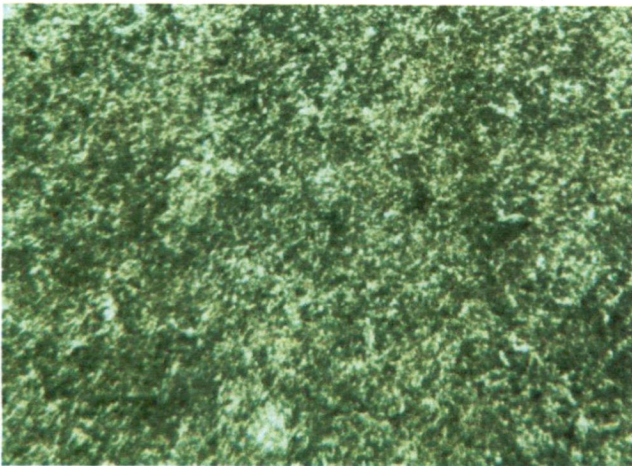
(a) Weld metal (magnification 25×)
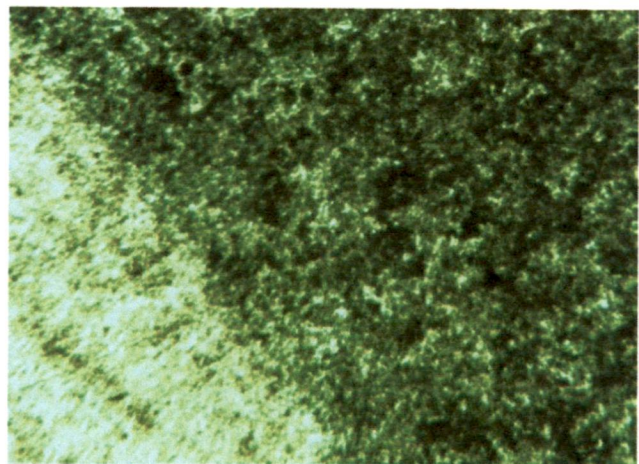
(b) HAZ (magnification 25×)
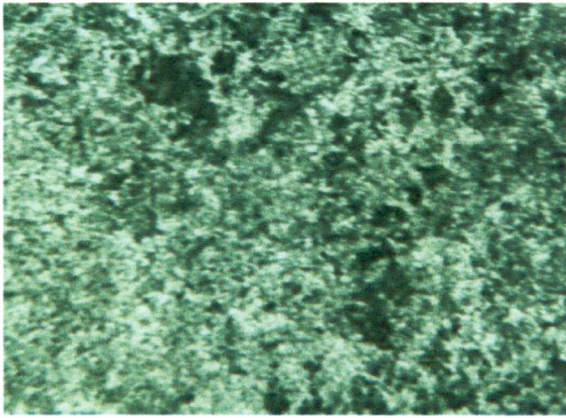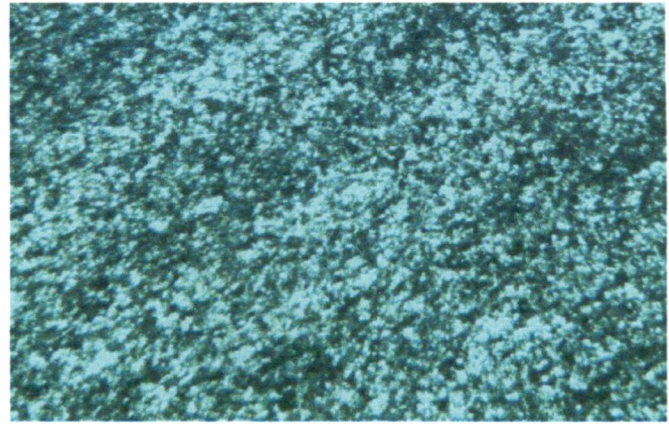
(c) HAZ (magnification 25×)   (d) BM (magnification 25×)

Figure 5.1: Microstructre of Different Regions Along the Weld

5.1.1 After 1hr PWHT the Microstructures of WM, BM and HAZ:

In HAZ maximum hardness is observed in as-welded condition. This is due to the presence of lath martensite.
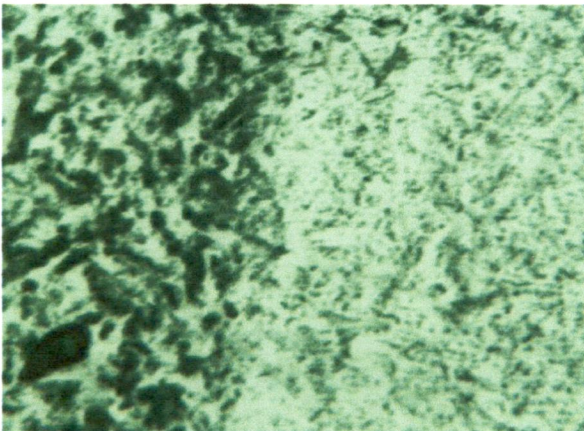
(a) BASE+WELD (magnification 100×)   (b) HAZ (magnification 50×)
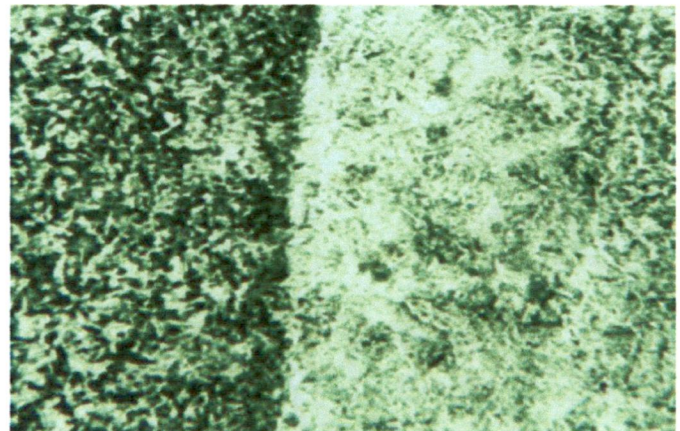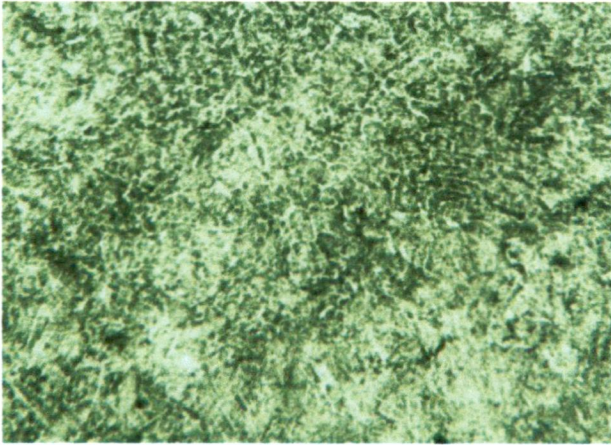
(c) WELD (magnification 25×)
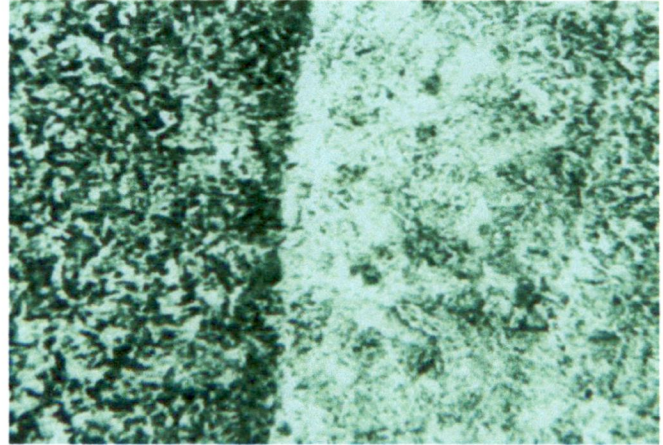
(d) HAZ (magnification 25×)
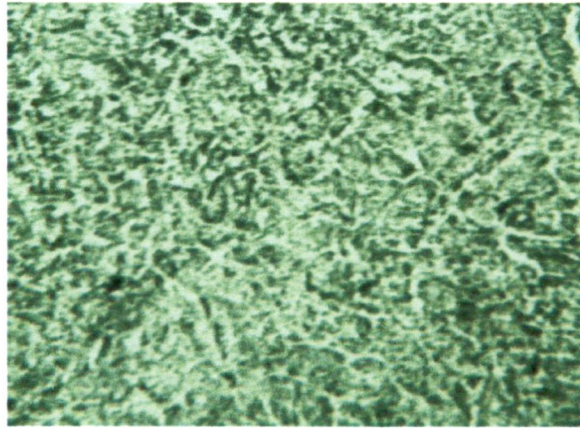
(e) WELD (magnification 50×)

Figure 5.2: Microstructre of Different Regions Along the Weld after PWHT

5.2 Hardness Test

The hardness test has been carried out to find out the hardness distribution in the Weld Metal HAZ as well as in the Base Metal at different location and it is observed that average hardness is in HAZ is more than Weld metal and Base Metal due to the work hardening in HAZ during the Welding.

The data found during the hardness test is tabulated below in Table 5.1 and with the help of these data various graphs have been plotted further, to study the hardness distribution at different locations along the weld metal.

Table 5.1 Hardness Test Results

S. No.	Distance From Weld Centre/mm	Location	Hardness /HVN
1	-10	Base metal	197
2	-9	Base metal	181
3	-8	Base metal	199
4	-7	Base metal	187
5	-6	Base metal	254
6	-5	Weld metal	232.5
7	-4	Weld metal	297
8	-3	Weld metal	285
9	-2	Weld metal	314
10	-1	Weld metal	297
11	0	Weld centre	280
12	1	Weld metal	309
13	2	Weld metal	241
14	3	Weld metal	311
15	4	Weld metal	315.5
16	5	Base metal	264
17	6	Base metal	230
18	7	Base metal	250
19	8	Base metal	197
20	9	Base metal	199
21	10	Base metal	181
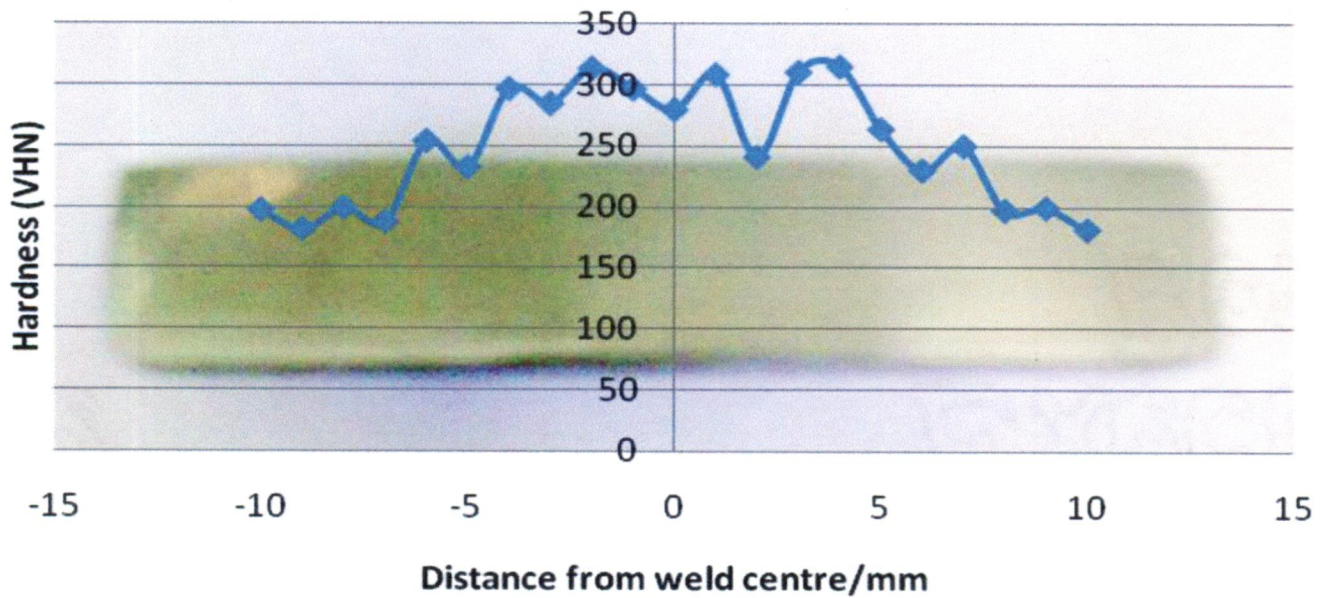
Figure 5.3: Hardness Distributions along the Weld

5.2.1 Hardness profile after 1 hr post weld heat treatment:

It is observed that after 1 hr post weld heat treatment on welded sample increasing hardness is reduced. In Weld metal more hardness is observed in as-welded condition. This is due to the precipitation of carbides.

Table 5.2 Hardness Test Results after PWHT

S. No.	Distance From Weld Centre/mm	Location	Hardness /HVN
1	-10.2	Base metal	180
2	-9.2	Base metal	171
3	-8.2	Base metal	181
4	-7.2	Base metal	187
5	-6.2	Base metal	160
6	-5.2	Weld metal	199
7	-5	Weld metal	176
8	-4	Weld metal	280
9	-3	Weld metal	297
10	-2	Weld metal	285

11	-1	Weld centre	269
12	0	Weld centre line	250
13	1	Weld metal	285
14	2	Weld metal	264
15	3	Weld metal	251
16	4	Weld metal	264
17	5	Weld metal	251
18	5.2	Weld metal	221
19	6.2	Base metal	193
20	7.2	Base metal	170
21	8.2	Base metal	181
22	9.2	Base metal	167.5
23	10.2	Base metal	172
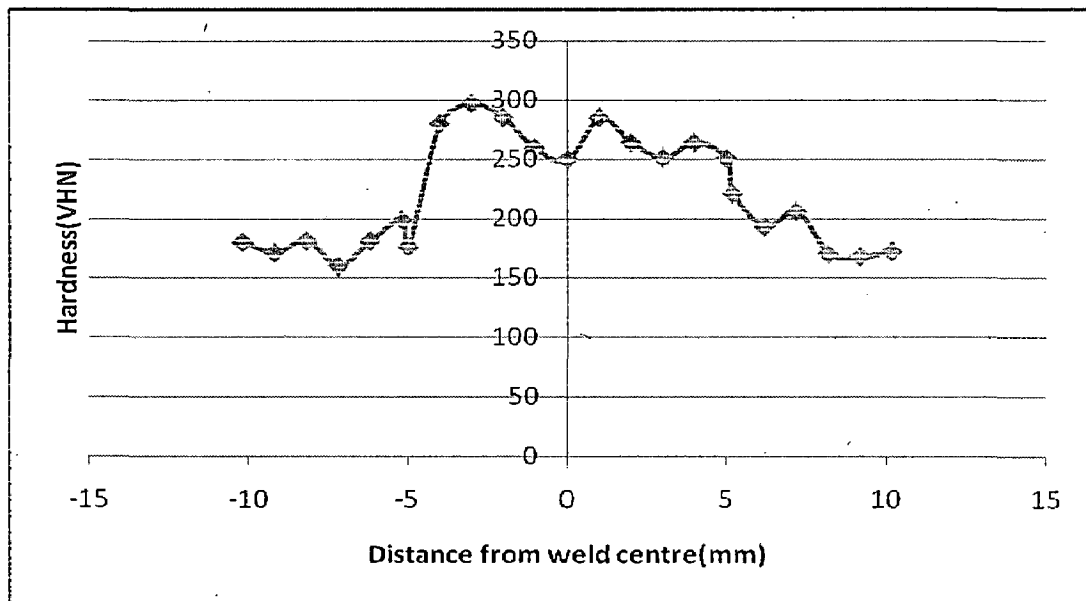
Figure5.4: Hardness Distributions along the Weld after PWHT

5.3 Tensile Test

Tensile test has been performed to find out the various mechanical properties like ultimate tensile strength, Yield strength and percentage elongation of base metal as well as weld metal.

Four tensile samples were tested using universal testing machine and stress strain curve for these three samples has been plotted as a result of the test.

Based on the data obtained, using the stress strain curve and with further calculations, a comparison of the mechanical properties of the base metal and weld metal is done and it was observed that weld metal is stronger than the base metal as the mechanical properties like ultimate tensile strength, Yield strength and percentage elongation are significantly higher than that of base metal

A. Parameter1

Welding current: 130A

Welding voltage: 24

Table 5.3: UTS, YS and % elongation of BM and WM

S.NO	MAX.LOAD (KN)	UTS (MPa)	LOAD at YIELD POINT(KN)	YIELD STRESS (MPa)	% ELOGATION	LOCATION OF FAILURE
1	16.3	576.37	10.3	364.21	20.16	WM
2	16	565.77	10	352.61	20.88	BM
3	16.2	572.84	10.5	371.28	21.22	WM
4	16.1	569.30	10.4	367.75	20.44	BM
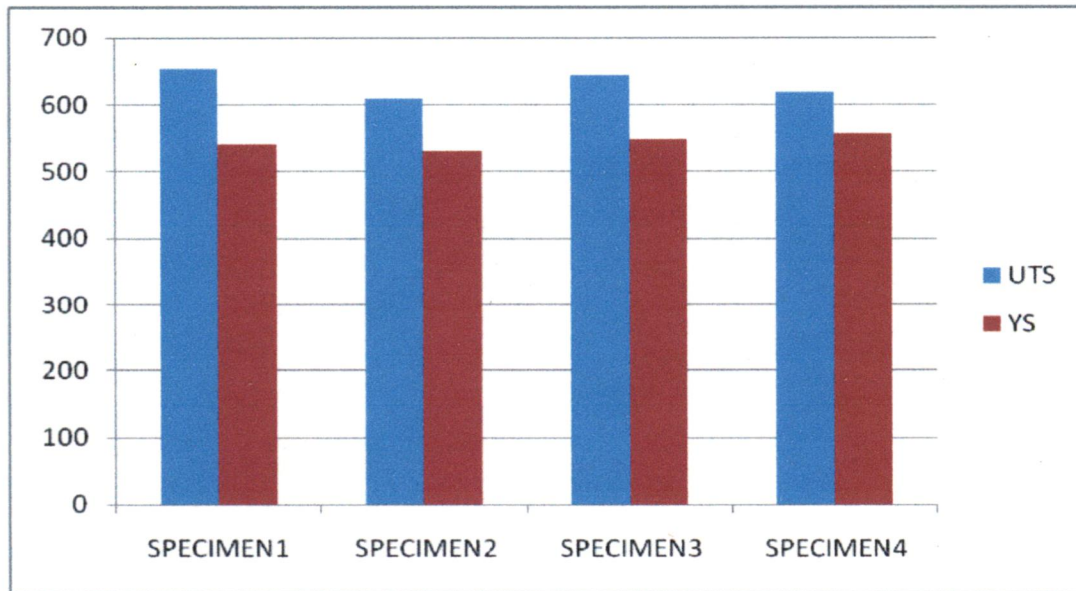
Figure5.5: Mechanical Properties of Base Metal and Weld Metal

REMARKS:

➢ The Ultimate Tensile Strength of **BM**=(565.77+569.30)/2=**567.53 MPa**

➢ The Ultimate Tensile Strength of **WM**=**574.61 MPa**

➢ Yield stress of **WM**= 367.74MPa

B. Parameter2

Welding current: 150A

Welding voltage: 24

Table 5.4: UTS, YS and % elongation of BM and WM (Parameter 2)

S.NO	MAX.LOAD (KN)	UTS (MPa)	LOAD at YIELD POINT(KN)	YIELD STRESS (MPa)	% ELOGATION	LOCATION OF FAILURE
1	16.1	569.30	10.1	357.14	19.35	WM
2	16.2	572.84	10.5	371.28	21.22	WM

REMARKS:

> The Ultimate Tensile Strength of WM=(569.30+572.84)/2=**571.07 MPa**

> Yield stress of WM= **364.21MPa**

C. Parameter3

Welding current: 170A

Welding voltage: 24V

Table 5.5: UTS, YS and % elongation of BM and WM (Parameter3)

S.NO	MAX.LOAD (KN)	UTS (MPa)	LOAD at YIELD POINT(KN)	YIELD STRESS (MPa)	% ELOGATION	LOCATION OF FAILURE
1	16	565.77	10	353.60	18.74	WM
2	15.9	562.23	10.2	360.68	18.55	WM

REMARKS:

> The Ultimate Tensile Strength of WM=(565.77+562.23)/2= **564MPa**

> Yield stress of WM= 357.14MPa

5.3.1 Comparison of Ultimate tensile strength, Yield strength of all the three parameters:
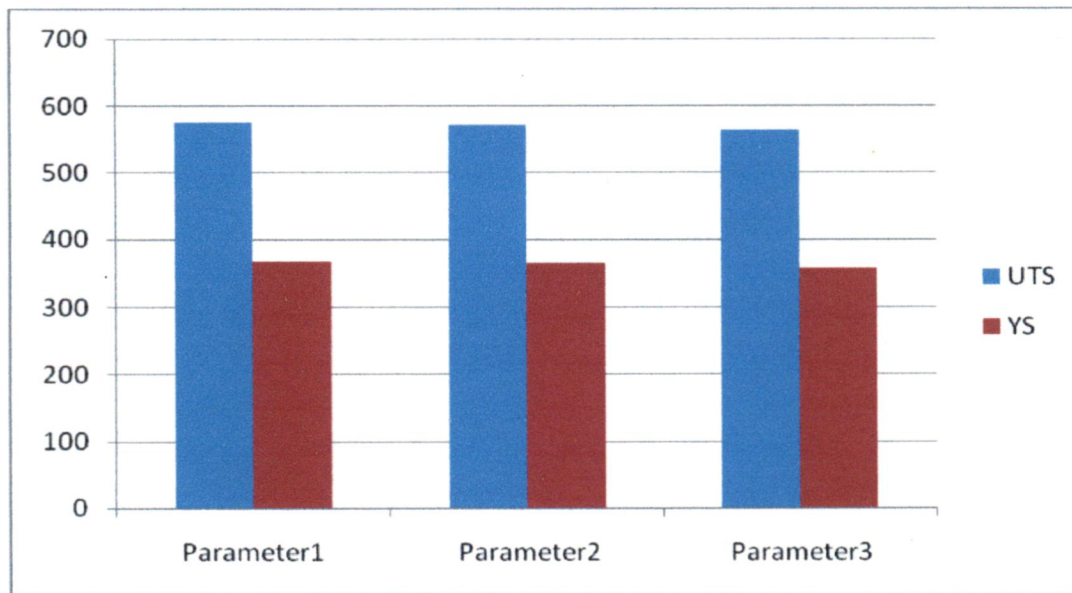
Fig 5.6: Combined Graph Between all three Parameters

5.4 Microanalysis of Fracture Surface of Tensile Tested Specimens Using SEM

The result obtained from electron microscopy (SEM) of fracture surface of different specimens of tensile test, show the base metal as well the weld metal are fractured in ductile manner. Fracture began at the centre of the specimens and then extends towards the outer surface by a shear separation.

5.4.1 Specimen 2& 4(Fracture from Base Metal)

As the both the specimen 2 & 4 were fractured from the base metal, therefore analysis of any of these two specimens will be enough to characterize the morphology of base metal fracture mode. The micrograph (Fig.5.7) show that the fracture surface is in the form of dimples is the evidence of ductile fracture of base metal while the small hole indicates the availability of more strain before fracture.
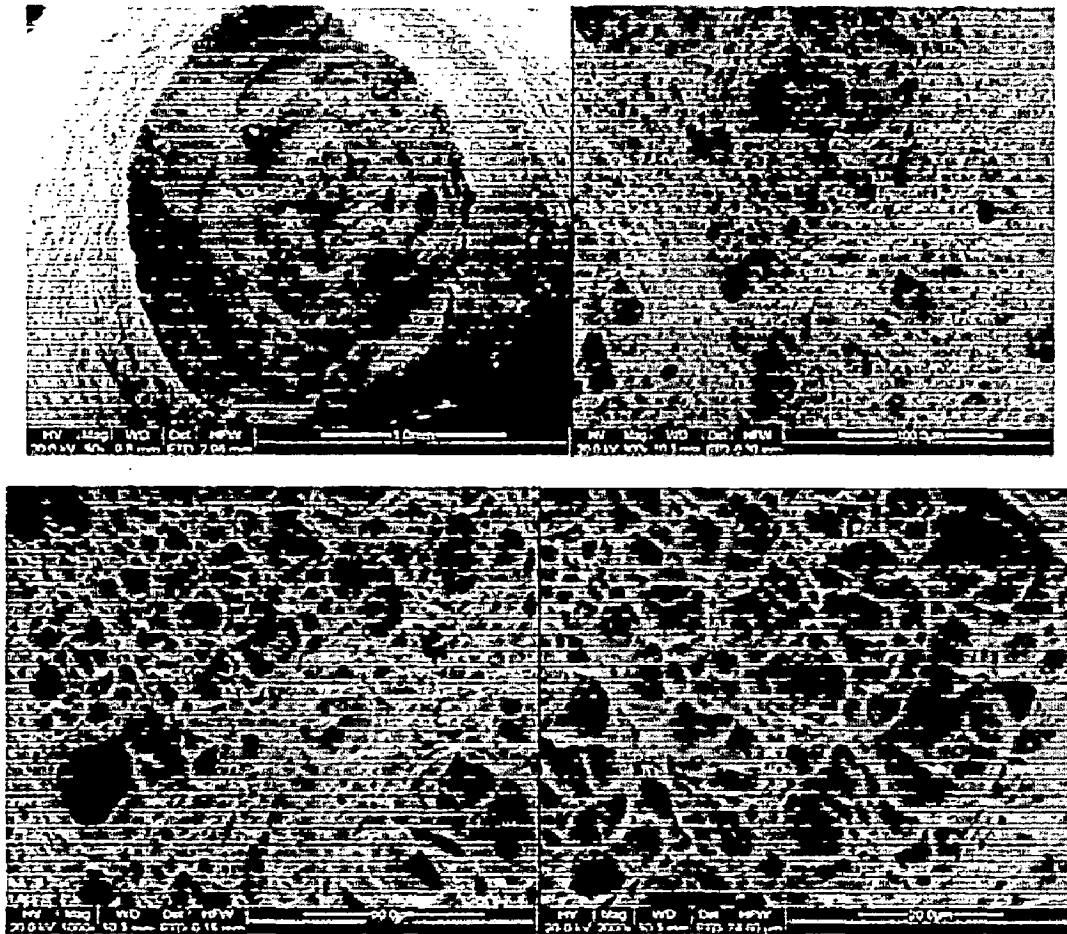
Figure 5.7: Scanning Electron Micrograph of Fracture Surface of Weld Metal

5.4.2 Specimen (Fractured from Weld Metal)

The scanning electron micrograph of the weld joint depicts the ductile fracture of the weld metal as fine dimples like fractured surface was observed.
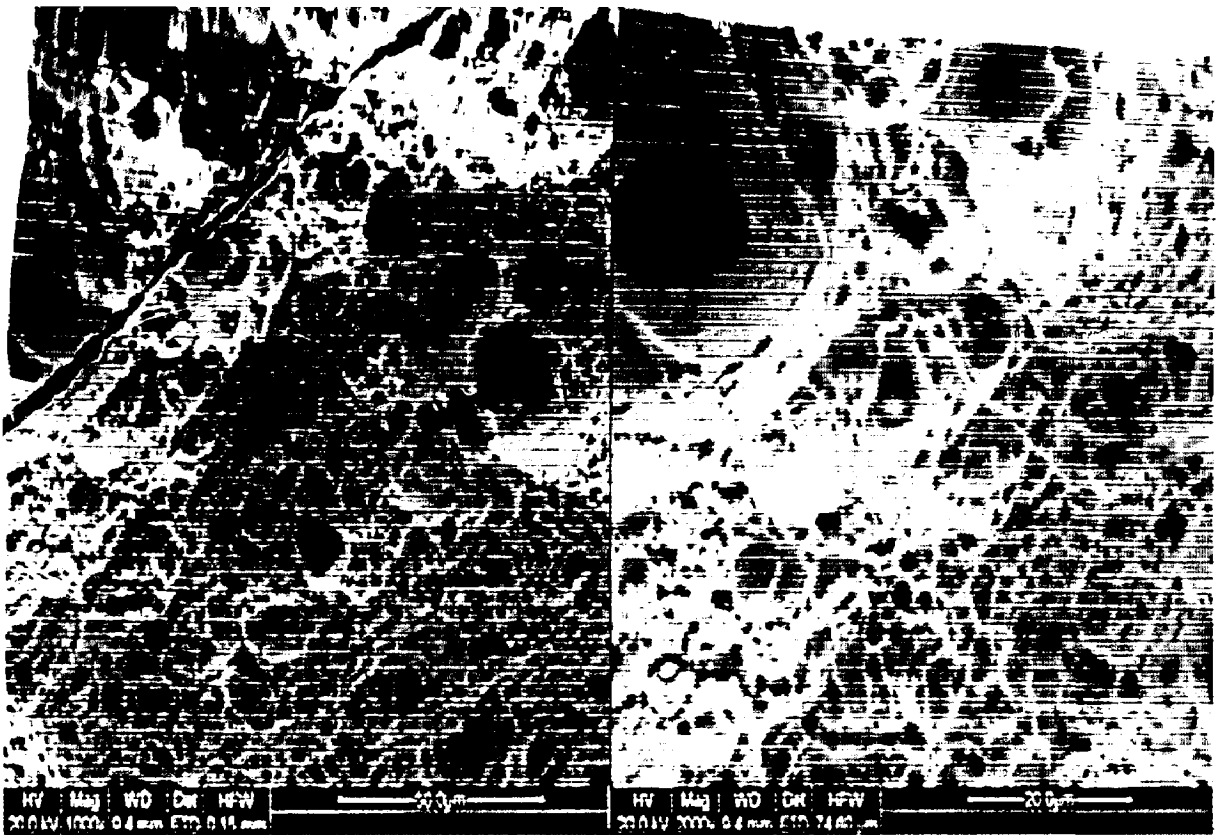
Figure5.8: Scanning Electron Micrograph of Fracture Surface of Weld Metal

52

5.5 EDAX Analysis of Weld Metal

EDAX analysis of weld metal has been performed to determine the composition of alloying element at a particular location in the weld metal. E-DAX analysis is focused on weld metal and the compositional variations are studied in as welded conditions. It is concluded that these variations will change the mechanical and microstructural properties.
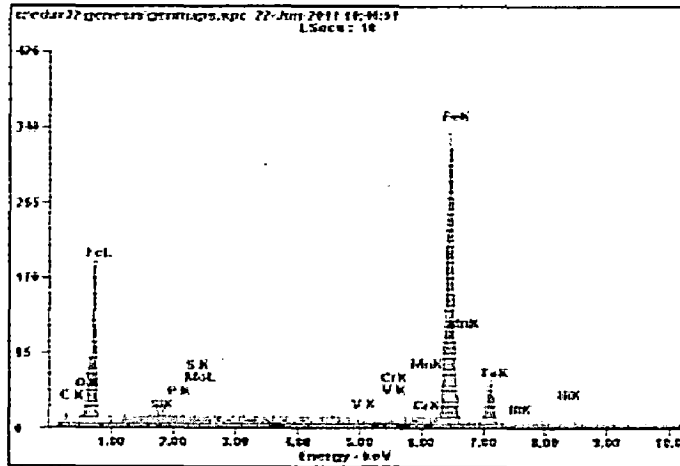
Element	Wt%	At%
CK	07.33	25.85
OK	01.96	05.19
SiK	01.18	01.79
PK	00.81	01.11
MoL	04.21	01.86
SK	00.00	00.00
VK	00.49	00.41
CrK	00.88	00.72
MnK	01.93	01.49
FeK	80.99	61.43
NiK	00.21	00.15
Matrix	Correction	ZAF
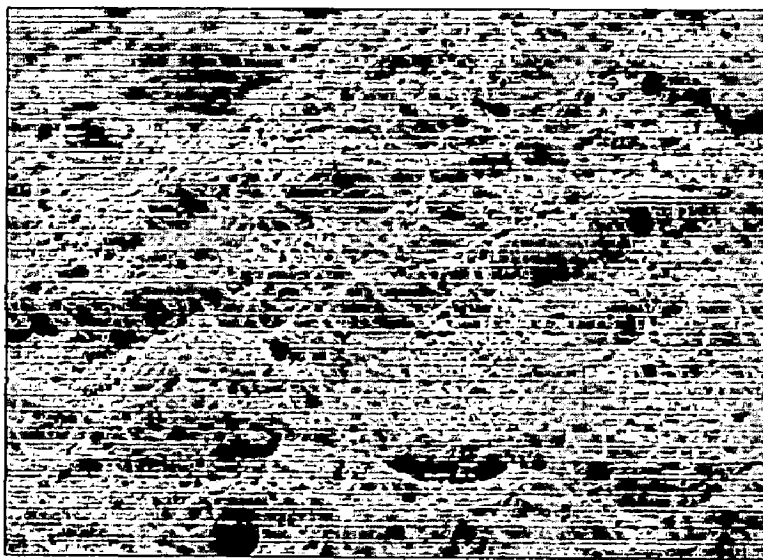
Figure 5.9: Elemental Distribution of Alloying Element in Weld

5.6 Impact Test

Charpy V-notch impact test is conducted on specimens in welded condition to determine the impact toughness. The notch is made in weld metal in transverse direction to the weld deposit. Table shown the toughness values at different weding parameter:

Table 5.6 Toughness reading at different welding parameter:

Parameters	Absorbed energy (J)
Parameter1	30
Parameter2	26
Parameter 3	24

5.7 Result and discussions for hot corrosion studies

Hot corrosion test is focused on base metal and weld metal. The hot corrosion test is carried at temperature of 900^0C in air environments. The result are characterized by weight change measurements, visual observations etc.

5.7.1 Weight change measurements:

Weight change measurements are recorded for Base metal and weld metal exposed to air oxidation. Graphs are plotted for weight gain vs time expressed in number of cycles.

The oxidation which occurred in air at temperature of 900^0C is shown by plotting a graph. On x-axis "number of cycles" and on y-axis "total weight gain" was taken. The air oxidation samples follow the parabolic kinetics when tested in hot corrosion. Base metal sample is highly affected as compared to weld metal which is confirmed by weight gain analysis.
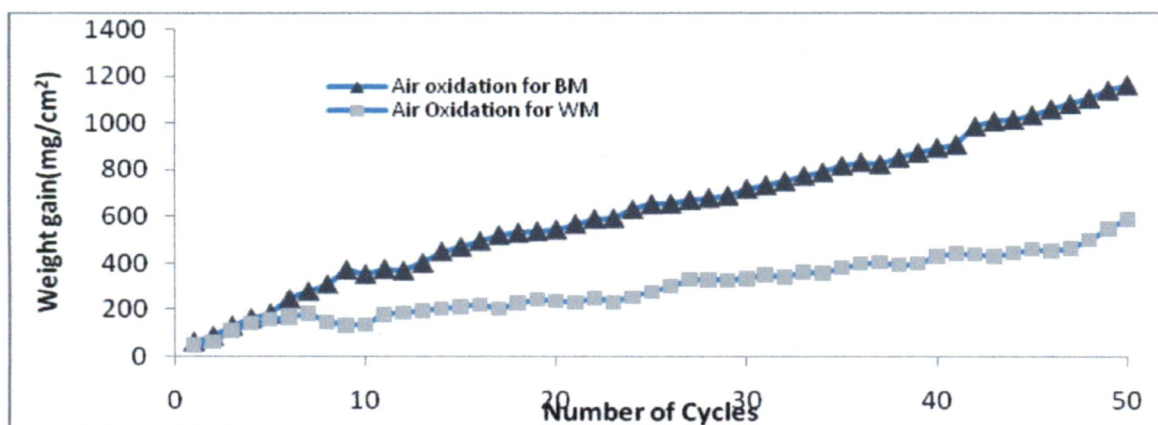
Fig. 5.10: Combination of graph of air oxidation in between WM & BM

CONCLUSIONS AND RECOMMENDATIONS

6.1 Conclusions

PWHT is used as a tool to impart mechanical and micro-structural properties of welded metal. The micro-structures in various regions of the weld joints like weld metal, HAZ, base metal and interface region show major changes in various mechanical properties in welded conditions and after PWHT, when examined under specified micro-structural conditions. These major changes have shown further changes in the mechanical properties.

Lath martensite is observed in HAZ as welded condition. The hardness is increased after one hour PWHT. The overall peak hardness is observed in HAZ portion next to that in weld metal and minimum in base metal.

It is also observed that the percentage of elongation and impact resistance increases when welding current decreases. From this result, it can be expected that there is another welding parameter applying which the UTS, YS and percentage elongation gains maximum values.

When hot corrosion test is done on un-welded sample, it is observed that corrosion rate is higher than that in base metal as comparison to weld metal.

6.2 Recommendations for future work

The present work gives a new direction to further improvement of mechanical, micro-structural properties and increasing resistance to Hot corrosion in boilers, pressure vessels, turbine parts, Diesel engine etc, in which Cr-Mo alloy steels are used. Following suggestions may be considered for future work.

➢ Some investigations can be focused on other boiler steels to determine the favourable PWHT time which gives better mechanical and micro-structural properties.

➢ Similar investigations can be focused on hot corrosion studies by comparing the different boiler grade materials.

➢ Further studies can be made to improve resistance to hot corrosion by applying coating like high-chromium, nickel chromium, NiCrAlY, Ni-20Cr, NiCrAlY-Al$_2$O$_3$ coating on super heater tubes used in boilers.

REFERENCES

1. *Metallurgical Guidebook for Fossil Power Plant Boilers.* EPRI, Palo Alto, CA: 2006. 1011912.

2. Kofstad, P., "High Temperature Corrosion", Elsevier Applied Science, London, pp.382-385, (1988).

3. Viswanathan, R., "Damage Mechanisms and Life Assessment of High Temperature Components." ASTM International, West Conshohocken, PA (1989).

4. Nawrocki, J.G., Dupont, J.N. and Robino, C.V. Post weld heat treatment response of simulated coarse-grained heat affected zones in a new ferritic steel. Journal of Metallurgical and Materials transactions, 32A, pp.2585-2594, (2001).

5. Klueh, R.L., The Effect of Carbon on 2.25 Cr-1 Mo Steel", Journal of nuclear materials 54 pp. 41-54, (1974).

6. Shiue, R.K., Lan, K.C., Chen, C., Toughness and austenite stability of modified 9Cr–1Mo welds after tempering, Materials Science and Engineering A287 pp. 10–16, (2000).

7. Sreenivasan, P.R., Charpy energy–lateral expansion relations for a wide range of steels, International Journal of Pressure Vessels and Piping 83, pp. 498–504. (2006).

8. Dhooge, A., Vinckier, A.,Reheat Cracking-a Review of Recent Studies, Int. J. Pres. Ves. & Piping 27, pp. 239-269, (1987).

9. Australian standard for Pressure Vessel Manufacturing, WTA, pp.1-10, (2003).

10. Makhlouf, K., Sidhom, H., Triguia, I., Braham, C.Z., Corrosion fatigue crack propagation of a duplex stainless steel X6 Cr Ni Mo Cu 25-6 in air and in artificial sea water, International Journal of Fatigue 25, pp. 167–179, (2003).

11. Choi, Y.H., Choi, S.Y., Socket weld integrity in nuclear piping under fatigue loading condition, Nuclear Engineering and Design 237, pp. 213–218.

12. Usman, A., Khan, A.N., Failure analysis of heat exchanger tubes, Engineering Failure Analysis, pp. 211-219 (2001).

13. Brown, T.B. Assessing the effect of thermal transients on the life of boiler plant, Babcock energy limited, SCOTLAND.

14. King, J.P., DB Riley, Worcester, Massachusetts, Recent experience in condition assessments of boiler header components and supports, Presented at the1996 ASME Pressure Vessels and Piping Conference July 21-26 (1996).

15. Paterson, I.R., Wilson, J.D., Use of damage monitoring systems for component life optimisation in power plant, International Journal of Pressure Vessels and Piping 79, pp. 541–547, (2002).

16. Takumi, T., Fumiko K., Toshihide, I., Hironori K., Crack propogation life prediction of a perforated plate under thermal, International Journal of Pressure Vessels and Piping 78 pp. 837–845 (2001).

17. Kerezsi, B.B., Kotousov, A.G., Price, J.W.H., Experimental apparatus for thermal shock fatigue investigations, International Journal of Pressure Vessels and Piping 77, pp. 425–434, (2000).

18. Ervin. E., Underwood, K.B., Fractal analysis of fracture surfaces ASM Hand Book ,Formely ninth edition ,metals hand book,volume-12

19. Wang, Y.Z., Ebtbhaj, K., Hardie, D., and Parkins, R.N. The behaviour of multiple stress corrosion cracks in a Mn-Cr and a Ni-Cr-MO-V steel: i-metallography, journal of Corrosion Science 37, pp. 1651-1675, (1995)

20. Hiromoto, S., Onodera, E., Chiba, A., Asami, K., Hanawa, T. Microstructure and corrosion behaviour in biological environments of the new forged low-Ni Co–Cr–Mo alloys, journal of Biomaterials 26, pp. 4912–4923, (2005).

21. Raman, S., Muddle, R. K., B. C. Role of high temperature corrosion in life assessment and microstructural degradation of Cr-Mo steel weldments, International Journal of Pressure Vessels and Piping 77, pp.117-123 (2000).

22. Andijani, I., Malik A.U., Sulfur and vanadium induced hot corrosion of boiler tubes, Presented at "Chemistry & Industry" Conference, King Saud University, Riyadh, on 11 to 15 Dec., 2004.

23 Pardo, Merino, A., Coy, M. C., Viejo, A.E., Arrabal, F., Matykina, R., Pitting, E., Corrosion behaviour of austenitic stainless steels – combining effects of Mn and Mo additions, journal of Corrosion Science 50, pp. 1796–1806 (2008).

24. Smith, B. J., Erskine, C. I., Hartranft, R. J., Marder, A. R., High- Temperature Corrosion-Fatigue (Circumferential) Cracking life Evaluation Procedure for low Alloy Cr-Mo) Boiler Tube Steels, Lehigh University, Bethlehem, PA 18025.

25. Swindeman, R.W., Santella, M., Maziasz, P.J., Roberts, B.W., Coleman, K., Issues in replacing Cr–Mo steels and stainless steels with 9Cr–1Mo–V steel, International Journal of Pressure Vessels and Piping 81, pp. 507–512 (2004).

26. Aslanlar, S., Ogur, A., Ozsarac, U., Ilhan, E., Demir, Z., Effect of welding current on mechanical properties of galvanized chromided steel sheets in electrical resistance spot welding, Materials and Design 28, pp. 2–7 (2007).

27. Sidhu, T. S., Prakash, S., Agrawal, R. D., Hot corrosion and performance of nickel-based coatings , Current science, 90, pp. 41-47 (2006).

28. Rathnama, D. V., Nagarajan, R. Surface chemical studies of "hot corrosion life prediction model for marine gas turbine blades and guide vanes, pp. 1377-1383.

29. Smith, B. J., Marder, A. R., A Metallurgical Mechanism for Corrosion-Fatigue (Circumferential) Crack Initiation and Propagation in Cr-Mo Boiler Tube Steels, Materials characterization 33, pp. 45-50 (1994).

30. Kou, S., Welding Metallurgy, Second Edition, Wiley Interscience publications 2003

31. Panda, B., Balasubramaniam, R., Dwivedi, G., On the corrosion behaviour of novel high carbon rail steels in simulated cyclic wet–dry salt fog conditions, Corrosion Science 50, pp.1684–1692 (2008).

32. Mars G. Fontana. Corrosion Engineering Third Edition, Tata McGraw-Hill Publishing Company Limited, Chapter, pp.4, (2005).

33. Khanna, "High Temperature Oxidation Basics", introduction to High Temperature Oxidation and Corrosion, ASM International, U.S.A, 2002.

34.http://en.wikipedia.org/wiki/File:Babcock_and_Wilcox_boiler_%28Heat_Engines,_1913

35. http://en.wikipedia.org/wiki/File:Water_tube_boiler_schematic.png

36. *The Handbook of Comparative World Steel Standards, Second Edition.* DS67A. ASTM International, West Conshohocken, PA: 2002.

APPENDIX

Behaviour of Cr-Mo Base metal in Air at 900^{0}C

Sample   = Cr-Mo alloy steel in weld and heat treated condition

Furnace used   = Tubular furnace

Controller of furnace   = PID Temperature controller

Sample dimensions   = 10mm×9.88mm×5.9mm

Sample weight   = 4.564gms

Boat +sample weight after preheating = 48.017gms

Cycle of 1 hr heating at 900^{0}C and then cooling to 20 minutes and taking weight along with boat

Table1: Weight gain observations of Base metal sample in air

No of cycles	Sample+Boat wt(gms)	Wt (gain gms)	Remarks
1	48.087	0.061	Tong sound while cooling, upper layer is removed in form of powder
2	48.113	0.085	Sample colour turned to dark greyish
3	42.353	0.127	Cracking sound observed while cooling, small pores were observed
4	42.385	0.159	Oxide colour change to black

5	42.405	0.179	....
6	42.468	0.242	Thick carbon layer cracked at lower side small patches of oxide layer fallen out
7	42.501	0.275	....
8	42.531	0.305	While cooling small noise occurred
9	42.593	0.367	Avery thick layer of black colour oxide exploded with noise
10	42.574	0.348	All oxide layer was separated
11	42.597	0.371	Oxide layer is splashed
12	42.589	0.363	....
13	42.611	0.395	Black oxide at corner side was observed
14	42.660	0.444	....
15	42.680	0.464	While cooling small noise occurred
16	42.654	0.488	....
17	42.680	0.514	....
18	39.288	0.524	Whole surface observed as very

			rough
19	39.308	0.530	Very thick layer of black oxide got separated
20	39.327	0.537	Thick oxide layer formed separated from all side completely
21	39.351	0.561	....
22	39.373	0.583	More squeezing sound occurred while cooling
23	33.942	0.586	The second layer which was formed also got cracked
24	33.979	0.623	Oxide layer got separated
25	34.001	0.645	....
26	25.119	0.647	The new oxide layer which was found also got exploded
27	25.134	0.662	For a small portion plane greyish oxide layer formed
28	34.108	0.671	Oxide layer were separated

29	34.118	0.681	Loud noise occurred and oxide got detached from corner side
30	34.147	0.710	....
31	34.162	0.725	While cooling sound was observed
32	34.179	0.742	Oxide layer got separated
33	34.202	0.765	....
34	34.217	0.780	While cooling sound occurred and oxide layer got separated
35	34.245	0.808	....
36	34.259	0.822	....
37	34.278	0.814	....
38	34.304	0.840	Top layer fall down and new layers got exposed to atmosphere
39	34.326	0.862	....
40	34.348	0.884	....
41	34.362	0.898	....
42	34.438	0.974	....
43	34.460	0.996	....

44	34.466	1.002	Squeezing voice occurred
45	34.485	1.021	....
46	33.511	1.047	....
47	34.532	1.068	Metallic sound occurred while cooling
48	34.556	1.092	....
49	34.590	1.126	....
50	34.657	1.148	....

Behaviour of Cr-Mo Weld metal in Air at 900^{0}C

Sample   = Cr-Mo alloy steel in weld and heat treated condition

Furnace used   = Tubular furnace

Controller of furnace   = PID Temperature controller

Sample dimensions   = 10.1mm×10mm×5.9mm

Sample weight   = 4.648gms

Boat +sample weight after preheating = 54.285gms

Cycle of 1 hr heating at 900^{0}C and then cooling to 20 minutes and taking weight along with boat .

Table 2: Weight gain observation of weld metal sample in air

No of cycles	Sample+Boat wt(gms)	Wt (gain gms)	Remarks
1	54.318	0.033	Tong sound while cooling, upper layer is removed
2	54.334	0.049	Sample colour turned to dark greyish. Cracks on bubbled surface layer
3	54.347	0.062	Cracking sound while cooling
4	54.397	0.112	Oxide colour changes to black
5	54.426	0.141	....
6	54.443	0.158	Thick carbon layer cracked with occurring of noise
7	54.443	0.168	....
8	54.460	0.185	While cooling small noise occurred
9	54.423	0.148	A very thick layer a black colour oxide exploded with noise
10	54.409	0.134	All oxide layer was separated

11	54.412	0.137	While cooling whole oxide layer formed
12	54.453	0.178	....
13	54.463	0.188	Black oxide at corner side was observed
14	54.472	0.197	....
15	54.480	0.205	While cooling small noise occurred
16	54.487	0.212	Oxide layer removed while cooling
17	54.497	0.222	....
18	54.478	0.203	Oxide layer separated by explosion and whole surface observed very rough
19	54.506	0.231	Very thick layer of black oxide got separated
20	54.519	0.244	Thick oxide layer formed from all sides
21	54.515	0.240	....
22	54.508	0.233	Little bit sound occurred while cooling
23	54.527	0.252	The second layer which was formed

			also got cracked
24	54.509	0.234	Oxide layer got separated with large sound
25	54.531	0.256	....
26	54.555	0.280	The new oxide layer was formed
27	54.578	0.303	Greyish oxide layer formed
28	54.610	0.335	Oxide layer from side of more thickness were separated
29	54.607	0.332	Loud noise occurred
30	54.605	0.330	....
31	54.684	0.339	While cooling sound was observed and thin layer of oxides formed
32	54.701	0.356	Oxide layer got separated
33	54.689	0.344	While cooling sound occurred
34	54.712	0.367	....
35	54.770	0.362	....

36	54.730	0.385	Oxide layer got removed
37	54.748	0.403	…………………..
38	54.753	0.408	Top layer fall down and new layers formed
39	54.742	0.397	…………………..
40	54.748	0.403	…………………..
41	54.773	0.434	…………………..
42	54.785	0.446	…………………..
43	54.781	0.442	…………………..
44	54.773	0.434	A voice occurred, water evaporated very rapidly
45	54.787	0.448	…………………..
46	54.804	0.465	…………………..
47	54.797	0.458	Metallic sound occurred while cooling
48	54.809	0.470	…………………..
49	54.814	0.505	…………………..
50	54.862	0.553	…………………..